



# CHORUS

This is the accepted manuscript made available via CHORUS. The article has been published as:

## Rydberg-atom-mediated nondestructive readout of collective rotational states in polar-molecule arrays

Elena Kuznetsova, Seth T. Rittenhouse, H. R. Sadeghpour, and Susanne F. Yelin

Phys. Rev. A **94**, 032325 — Published 27 September 2016

DOI: [10.1103/PhysRevA.94.032325](https://doi.org/10.1103/PhysRevA.94.032325)

# Rydberg atom mediated non-destructive readout of collective rotational states in polar molecule arrays

Elena Kuznetsova,<sup>1,2</sup> Seth T. Rittenhouse,<sup>3</sup> H. R. Sadeghpour,<sup>4</sup> and Susanne F. Yelin<sup>4,5,6</sup>

<sup>1</sup>*Rzhanov Institute of Semiconductor Physics, Novosibirsk, 630090, Russia*

<sup>2</sup>*Russian Quantum Center, 100 Novaya Street, Skolkovo, Moscow region, 143025, Russia*

<sup>3</sup>*Department of Physics, The United States Naval Academy, Annapolis, MD 21402, USA*

<sup>4</sup>*ITAMP, Harvard-Smithsonian Center for Astrophysics, 60 Garden Street, Cambridge, MA 02138, USA*

<sup>5</sup>*Department of Physics, University of Connecticut, 2152 Hillside Road, Storrs, CT 06269*

<sup>6</sup>*Department of Physics, Harvard University, 17 Oxford Street, Cambridge, MA 02138, USA*

We analyze the possibility to exploit charge-dipole interaction between a single polar molecule or a 1D molecular array and a single Rydberg atom to read out molecular rotational populations. We calculate the energy shift of a single Rb(60s) atom interacting with a single KRb or RbYb molecule in their lowest two rotational states. At atom-molecule distances, relevant to trapping of molecules in optical lattices, the Rydberg electron energy shifts conditioned on the rotational states, are of the order of several MHz. Atom excitation to a Rydberg state and detection of atomic fluorescence conditioned on a rotational state preserves the molecule, making our scheme a non-destructive measurement of the rotational state. Similarly, a 1D array of polar molecules can shift the electron energy of a blockaded Rydberg superatom. We consider a scheme to read out the molecular array collective rotational states using the conditioned Rydberg energy shifts, and numerically analyze a system with 3 and 5 KRb or RbYb molecules interacting with Rb(60s) superatom.

PACS numbers:

## I. INTRODUCTION

Ultracold polar molecules placed in a periodic array represent an attractive setup for quantum computation [1] and simulation of strongly correlated many-body systems due to the ability to interact via anisotropic and long-range electric dipole-dipole interaction. Such a system can be used to simulate quantum magnetism [2], exotic topological states [3], and complex many-body entanglement [4]. First experimental observations of spin exchange processes between the dipoles of KRb molecules in a 3D optical lattice have been reported recently [5], and a similar effect in a Cr gas of magnetic dipoles [6].

Typically a spin-1/2 particle or a qubit is encoded in two rotational molecular states and an initial many-body state becomes strongly entangled due to the interaction. The state of such entanglement will need to be read out to extract useful information about the system. One main challenge for the current ultracold molecule setups is that there exists no reliable scheme for readout which does not lead to loss of molecules.

In this work, we propose an elegant approach to non-destructively read out the rotational excitations in a mesoscopic ensemble of molecular array. We consider a linear or a ring 1D array of molecules interacting with a 1D array or cloud of neutral atoms in a symmetric state with a single Rydberg excitation (superatom). We show that in this setup it is possible to measure total populations of collective rotational states without losing or destroying the molecules.

Most current methods for molecular state readout, such as inverse STIRAP (stimulated Raman adiabatic passage) combined with Feshbach dissociation for alkali dimers [5] and REMPI (resonantly enhanced multiphoton

ionization) [7], are destructive. Non-destructive readout of rotational states of a single molecular ion interacting with an atomic ion by Coulomb interaction has been reported recently [8]. In previous work [9] we proposed a technique to read out populations of rotational molecular states of a single neutral polar molecule relying on its interaction with a nearby Rydberg atom [10, 11]. This interaction shifts the states of the combined molecule-Rydberg atom system depending on the rotational state, allowing conditional excitation and fluorescence of the atom, realizing readout of rotational states conserving the molecule.

There is strong and growing interest in manipulating states of few- to many-body systems using their interaction with a single ancilla system. Examples include control of environment nuclear spins by a single electron spin in diamond NV centers [12] or in quantum dots [13], including polarization [14], superradiance [15], squeezing [16], and quantum metrology [17]. Recently these ideas have been extended to atomic systems, using Rydberg states for spectroscopy [18, 19] or topological measurements [20]. Here we propose using Rydberg atoms to read out collective states of mesoscopic systems of polar molecules.

Due to a lack of cycling transitions, non-destructive measurements of molecular states need auxiliary systems for readout, and our suggested path via Rydberg spectroscopy is akin to the technique of quantum logic spectroscopy [21]. Earlier [22], common mechanical oscillatory modes of an ion and a molecule were suggested for a similar task. The neutrality of Rydberg atoms and molecules, as in our setup, however, makes co-trapping and manipulation with external electric fields easier.

The paper is organized as follows. In Section II we

derive matrix elements of the Hamiltonian for the combined single molecule-single Rydberg atom system. In Section III we numerically calculate energy shifts of the rotational states of KRb and RbYb molecules interacting with Rb(60s) atom. In Section IV we analyze the interaction between a linear or a ring 1D array of molecules and a Rydberg superatom, placed either in a parallel commensurate 1D array or a dipole trap. In Section V we discuss readout of rotational states of a single molecule or an array of molecules using its interaction with a Rydberg atom. Finally, we conclude in Section VI.

## II. SINGLE ATOM - SINGLE MOLECULE INTERACTION

We envisage a setup shown in Fig. 1a where a 1D or 2D array of polar molecules is used to simulate a strongly correlated many-body quantum system. Each polar molecule represents a qubit or a spin-1/2, encoded in rotational states  $|\downarrow\rangle = |J=0, m_J=0\rangle$  and  $|\uparrow\rangle = |J=1, m_J=0\rangle$  or  $|\uparrow\rangle = |J=1, m_J=\pm 1\rangle$  [5]. Parallel to the molecular array there is an array with neutral atoms, which can be individually excited to Rydberg states to read out molecular states. Although a setup with two close lattices, one filled with molecules and another with atoms has yet to be realized, two parallel optical lattices filled with neutral atoms have been demonstrated recently [23].

The configuration for a single polar molecule interacting with a single Rydberg atom [10] is depicted in Fig. 1b: the molecule is a part of e.g. an array aligned along the X axis with its own Rydberg atom at a distance  $\rho$  from the X axis, placed at  $\Delta x = 0$ .

The Hamiltonian governing the single atom - single molecule system is given by

$$H = H_a + H_m + V_{e^- - M}, \quad (1)$$

where

$$H_a = \sum_{n,l,m} E_{nl} |nlm\rangle \langle nlm|$$

is the unperturbed Rydberg atom Hamiltonian at principal quantum numbers  $n$ , orbital angular momentum  $l$ , and a  $z$  projection of  $l$ ,  $m$ . (Electron spin mixing due to Rydberg electron spin-orbit and ground electron hyperfine interactions are not included [24]). We calculate interaction induced energy shifts of  $ns$  Rydberg states due to electron-molecule interaction  $V_{e^- - M}$  by including the  $ns$  and the nearest  $p$  and  $d$ , and  $f$  states, whose quantum defects are nonzero:  $|np\rangle$  and  $|(n-1)p\rangle$ ,  $|(n-1)d\rangle$  and  $|(n-2)d\rangle$ , and  $|(n-3)f\rangle$ . The corresponding unperturbed energies of Rydberg states are  $E_{nl} = -1/2(n - \mu_l)^2$  in atomic units,  $\mu_l$  is the quantum defect (for Rb  $\mu_s = 3.13$ ,  $\mu_p = 2.65$ ,  $\mu_d = 1.34$ ,  $\mu_f = 0.016$ ). As a typical example, we use for our simulations  $|ns\rangle = |60s\rangle$ ,  $|np\rangle = |60p\rangle$ ,  $|(n-1)p\rangle = |59p\rangle$ ,

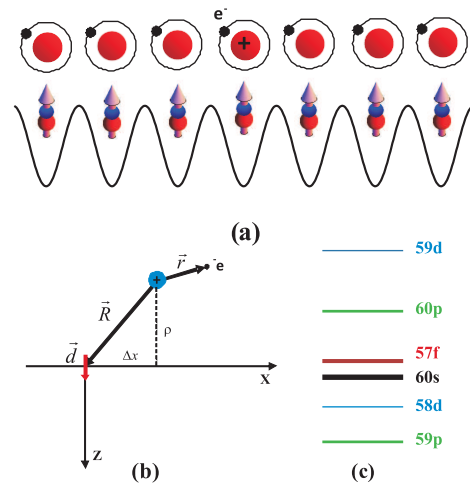


FIG. 1: (a) Setup geometry: a 1D or 2D array of polar molecules, interacting via charge-dipole interaction with nearby Rydberg atoms, placed in a parallel array; (b) a polar molecule with a dipole moment  $\vec{d}$  interacts with a Rydberg atom. The distance between the X axis and the Rydberg core is  $\rho$ , the distance between the molecule and the vertical line connecting the core and the X-axis is  $\Delta x$ ; (c) Level scheme of Rydberg states of Rb near 60s state, taken into account in the calculations (not to scale). The energy splittings are:  $E_{60p} - E_{60s} = 17.06$  GHz,  $E_{60s} - E_{59p} = 18.75$  GHz,  $E_{59d} - E_{60s} = 27.46$  GHz,  $E_{60s} - E_{58d} = 7.79$  GHz,  $E_{57f} - E_{60s} = 4.07$  GHz.

$|(n-1)d\rangle = |59d\rangle$ ,  $|(n-2)d\rangle = |58d\rangle$  and  $|(n-3)f\rangle = |(n-3)f\rangle = |57f\rangle$  states. The corresponding atomic level scheme with energy splittings is shown in Fig. 1c. In Rb, the  $(n-3)l$  with  $l > 3$  degenerate manifolds are known to produce considerable mixing of the Rydberg energies, leading to formation of large permanent dipole moments in the polyatomic molecules [25]. To be able to manage the size of the Hamiltonian matrix, we do not take account of these degenerate manifolds. Since the inclusion of such terms should yield more pronounced shifts this means that we rather underestimate the interaction induced resolution of rotational qubits. The  $H_m = BJ^2$  Hamiltonian describes a rigid rotor molecule with states  $|J, m_J\rangle$  with  $H_m|J, m_J\rangle = BJ(J+1)|J, m_J\rangle$  and rotational constant  $B$ , and  $V_{e^- - M} = \frac{e\vec{d}\cdot\vec{R}}{R^3} - \frac{e\vec{d}\cdot(\vec{R}-\vec{r})}{|\vec{R}-\vec{r}|^3}$  is the charge-dipole interaction between the Rydberg atom ionic core and electron and the molecule, where  $\vec{d}$  is the molecular dipole moment,  $\vec{R}$  is the distance between the Rydberg core and the molecule, and  $\vec{r}$  is the distance between the core and the Rydberg electron. The molecular permanent dipole moment of our two example molecules is chosen to be below the Fermi-Teller critical value of  $d_{cr} = 1.63$  D [10].

Next we calculate the shifts of the states  $|nlm\rangle|\downarrow\rangle = |nlm\rangle|J=0, m_J=0\rangle$  and  $|nlm\rangle|\uparrow\rangle = |nlm\rangle|J=1, m_J=0, \pm 1\rangle$  of the combined atom-molecule system. For that we additionally take into ac-

count unperturbed states  $|nlm\rangle |J = 2, m_J = 0, \pm 1, \pm 2\rangle$ . The matrix elements of  $H_a$ ,  $H_m$  and  $V_{e-M}$  are given by:

$$\begin{aligned}
\langle J, m_J | \langle n l m | H_a | n' l' m' \rangle | J', m'_J \rangle &= \\
&= -\frac{1}{2(n - \mu_l)^2} \delta_{n,n'} \delta_{l,l'} \delta_{m,m'} \delta_{J,J'} \delta_{m_J,m'_J}, \\
\langle J, m_J | \langle n l m | H_m | n' l' m' \rangle | J', m'_J \rangle &= \\
&= BJ(J+1) \delta_{n,n'} \delta_{l,l'} \delta_{m,m'} \delta_{J,J'} \delta_{m_J,m'_J}, \\
\langle J, m_J | \langle n l m | V_{e-M} | n' l' m' \rangle | J', m'_J \rangle &= \\
&= \langle J, m_J | e\vec{d} \cdot | J', m'_J \rangle \frac{\vec{R}}{R^3} \delta_{n,n'} \delta_{l,l'} \delta_{m,m'} \\
&\quad - \langle J, m_J | e\vec{d} \cdot | J', m'_J \rangle \langle n l m | \frac{\vec{R} - \vec{r}}{|\vec{R} - \vec{r}|^3} | n' l' m' \rangle.
\end{aligned} \tag{2}$$

Energies of the states of the combined atom-molecule system can be obtained by diagonalizing the Hamiltonian Eq. (1). Details of the calculation of matrix elements Eq. (2) are given in App. A.

### III. NUMERICAL RESULTS FOR ENERGIES OF KRb-Rb(60s) AND RbYb-Rb(60s) SYSTEMS

In this section we numerically calculate the energies of the combined single atom-single molecule system, shown in Fig. 1b, for the case  $\Delta x = 0$  and atom-molecule distances  $\rho \sim 300 - 600$  nm, corresponding to a period of a typical optical lattice.

We consider two polar molecules KRb and RbYb of particular interest in the ultracold community. KRb with a permanent electric dipole moment and rotational constant of  $d = 0.566$  D [26] and  $B = 1114$  MHz [27], respectively, was the first polar molecule produced in the ground rovibrational electronic  $^1\Sigma^+$  state at ultracold temperatures [28] and is the most experimentally well-mastered at the moment. RbYb with  $d \approx 1$  D [29] and  $B = 353$  MHz [29] belongs to the family of open-shell molecules with  $^2\Sigma^+$  ground electronic state, and is actively studied experimentally [30, 31] and theoretically [32] towards the goal of producing ground rovibrational state molecules. Polar molecules with the  $^2\Sigma^+$  ground state have both an electric and a magnetic dipole moment and are attractive for applications in quantum computation [33] and simulation of lattice-spin models [34]. Other candidate molecules with subcritical dipoles, to which the readout method is applicable, include RbCs ( $d = 1.25$  D [35],  $B = 490$  MHz [36]) and LiNa ( $d = 0.566$  D,  $B = 11.3$  GHz [37]) among alkali dimers, and a number of alkali metal-alkaline earth diatoms such as NaSr ( $d = 0.63$  D,  $B = 1.89$  GHz [38]), KSr ( $d = 1.5$  D,  $B = 960$  MHz [38]), RbSr ( $d = 1.53$  D,  $B = 540$  MHz [38]), and NaCa ( $d = 1$  D,  $B = 2.49$  GHz [39]).

In RbYb, the unpaired electron spin couples to the Rb nuclear spin, resulting in hyperfine splitting of the

ground electronic state, which is expected to be close to the splitting of 6.835 GHz between  $F = 1$  and  $F = 2$  hyperfine states of Rb atom [31]. In the calculations RbYb is assumed to be in the ground electronic potential, corresponding to the lowest in energy  $F = 1$  hyperfine state. Rotational states of the ground state of RbYb are further split by a spin-rotation interaction  $\gamma_{SR} \vec{J} \vec{S}$ , whose coupling strength can be approximated as  $\gamma_{SR} = -2\Delta g_{\perp} B$  [40], where  $\Delta g_{\perp} = g_{\perp} - g_e$  is the deviation of the molecular g tensor component, perpendicular to a molecular axis, from the electron's value. The spin-rotation splittings have not been detected for  $J = 1$  rotational states of the last and second last bound vibrational levels of RbYb [41]. In this experiment the frequency resolution was  $\Delta f_{res} \approx 6$  MHz, limiting the spin-rotation constant to this value. The rotational constant for such high vibrational states was measured to be  $B(\nu = -1) \approx 30$  MHz, while for the ground vibrational state it is predicted to be  $B(\nu = 0) = 353$  MHz, setting an upper limit on the spin-rotation constant in the ground vibrational state  $\sim \Delta f_{res} B(\nu = 0) / B(\nu = -1) \approx 70$  MHz, provided  $\Delta g_{\perp}$  does not significantly vary with the vibrational number.

The effect of the spin-rotation splitting (not taken into account in the calculations) can be estimated in the following way: if  $|V_{e-M}| \ll 2B$  (see App. B), the energy shifts of the atom-molecule system can be approximated using perturbation theory as  $|\Delta E| \sim |V_{e-M}|^2 / 2B$ . The spin-rotation will modify the energy shifts as  $|\Delta E| \sim |V_{e-M}|^2 / (2B \pm \gamma_{sr}) \approx |V_{e-M}|^2 (1 \pm \gamma_{sr} / 2B) / 2B$ , where  $\gamma_{sr} / 2B \leq 0.1$ .

In Fig. 2a and Fig. 2b the energy shifts of the states  $|J = 0, m_J = 0\rangle$  and  $|J = 1, m_J = 0, \pm 1\rangle$ , are shown for KRb and RbYb, respectively, interacting with Rb( $ns = 60s$ ) state. The shifts are calculated with respect to unperturbed energies of the states  $E_{ns} + 2BJ(J+1)$ . Since in the ground atomic state  $|g\rangle$  the atom-molecule interaction is much weaker compared to Rydberg states, the energy shifts also give the frequency shifts of the transitions  $|g\rangle |J, m_J\rangle \rightarrow |ns\rangle |J, m_J\rangle$ . These states contain admixtures of other states of the order of  $\leq 0.7\%$ . We assume that the molecule and the atom are separated by distances  $\rho \sim 300 - 600$  nm, corresponding to a period of a typical optical lattice. At these distances and for relatively small dipole moments ( $d \leq 1$  Debye) of the molecules the interaction matrix elements between  $|ns\rangle |J = 0, m_J = 0\rangle$ ,  $|ns\rangle |J = 1, m_J = 0, \pm 1\rangle$  and other states are small compared to energy difference between the corresponding states (see App. B), which explains the small admixing of other states.

In Fig. 2b, one observes that for RbYb the splitting between the states  $|J = 0, m_J = 0\rangle$  and  $|J = 1, m_J = 0\rangle$  lies in the range  $\sim 6.5 - 1.2$  MHz for  $\rho \sim 400 - 600$  nm, and the states  $|J = 0, m_J = 0\rangle$  and  $|J = 1, m_J = \pm 1\rangle$  are split in the range  $\sim 3 - 0.6$  MHz. Due to a smaller permanent dipole moment of KRb and a larger rotational constant the splittings for KRb are smaller compared to the splittings for RbYb at the same  $\rho$ . Split-

tings of the order  $\sim 1$  MHz can be achieved for KRb for smaller  $\rho$ . As shown in Fig. 2a the states  $|J = 0, m_J = 0\rangle$  and  $|J = 1, m_J = 0\rangle$  are split by  $\sim 2.2 - 0.4$  MHz for  $300 \text{ nm} < \rho < 500 \text{ nm}$ , and the states  $|J = 0, m_J = 0\rangle$  and  $|J = 1, m_J = \pm 1\rangle$  are split by  $\sim 1.1 - 0.2$  MHz for the same range. The splittings are much larger than the width of Rb( $60s$ )  $\Gamma_{60s} \approx 1.644$  kHz, resulting from spontaneous emission, black-body radiation (BBR) induced decay, excitation and ionization and the width of the  $J = 1$  rotational state due to spontaneous emission and interaction with black-body radiation [42].

The convergence of the energy shifts with respect to the atomic and molecular basis states is discussed in App. C, where it is shown that for KRb the basis set of  $60s$ ,  $60p$ ,  $59p$ ,  $59d$ , and  $58d$  is required to obtain accurate numerical results. For RbYb on the other hand, even the smallest atomic basis set including only the  $60s$  state provides good agreement with the full atomic set. The effect of  $57f$  state is rather small for both KRb and RbYb, which is explained by the energy gap between the  $60s$  and  $57f$  states and small interaction matrix elements between these states. The effect of higher rotational states such as  $|J = 3, m_J = 0, \pm 1, \pm 2, \pm 3\rangle$  on the energy shifts of the  $J = 0$  and  $J = 1$  states was found to be negligible.

Finally, we discuss the effect of position fluctuations of both the molecule and the Rydberg atom during the interaction. Assuming that they are trapped in ground states of their harmonic traps, it is shown in App. D that the energy shifts of the states  $|ns\rangle |J = 0, m_J = 0\rangle$ ,  $|ns\rangle |J = 1, m_J = 0, \pm 1\rangle$  get an additional contribution  $\sim \Delta E_{ns, J, m_J} (a/\rho)^2$ , where  $a$  is the trap ground state wavefunction width, assumed equal for the atom and the molecule.

#### IV. N MOLECULES – RYDBERG SUPERATOM INTERACTION

What happens if  $N$  polar molecules interact now with Rydberg atoms? This section concerns a 1D array or cloud of atoms placed in parallel to  $N$  molecules. Basically, it is the same setup as in the previous section where only one atom–molecule pair was treated. Here, the laser beam that excites atoms to their Rydberg state interacts with all atoms simultaneously. Then, the *dipole blockade* [43] will ensure that exactly one collective Rydberg excitation (a superatom) will exist in the ensemble.

The superatom wavefunction will be a superposition of states with different single excited Rydberg atoms

$$|\Psi_{\text{atom}}\rangle = \frac{1}{\sqrt{N_a}} \sum_{j=1}^{N_a} e^{ik_x \text{Rydb} X_j} |g_1, \dots, g_{j-1}, r_j, g_{j+1}, \dots, g_{N_a}\rangle, \quad (3)$$

where  $N_a$  is the number of atoms,  $|g_j\rangle$  and  $|r_j\rangle$  denote  $j^{\text{th}}$  atom in the ground or Rydberg state and  $X_j$  its position along the array,  $k_x \text{Rydb}$  is the x component of the wavevector of the exciting laser field.

Next, we analytically and numerically calculate the energy shifts of the states of the combined interacting system of  $N$  molecules and a Rydberg superatom. Numerically the shifts can be obtained by diagonalizing the Hamiltonian of the combined system using the basis of superatom states with a range of Rydberg states, as was done in the previous section, and a set of collective molecular rotational states. Here, in order to simplify the calculations we use the smallest atomic basis set of the  $|r\rangle = |60s\rangle$  state for the superatom in diagonalizing the interaction Hamiltonian  $V_{e^- - M}$ . Then the interaction of  $i^{\text{th}}$  molecule with the atomic array takes the form:

$$\begin{aligned} \langle \Psi_{\text{atom}} | V_{e^- - M, i} | \Psi_{\text{atom}} \rangle &= \\ &= \frac{1}{N_a} \sum_{j=1}^{N_a} \langle r_j | V_{e^- - M, i} | r_j \rangle = \frac{1}{N_a} \sum_{j=1}^{N_a} V_{ji}, \end{aligned} \quad (4)$$

where  $V_{ji} = \langle r_j | V_{e^- - M, i} | r_j \rangle = \langle r_j | \frac{e\vec{d}_i \cdot \vec{R}_{ji}}{R_{ji}^3} - \frac{e\vec{d}_i \cdot (\vec{R}_{ji} - \vec{r})}{|\vec{R}_{ji} - \vec{r}|^3} | r_j \rangle$  and  $\vec{R}_{ji}$  is the vector connecting  $j^{\text{th}}$  atom to  $i^{\text{th}}$  molecule. In fact, one can see from Eq. (4) that interatomic coherences do not play a role and the same result can be obtained with a mixed atomic state described by a density matrix

$$\rho = \frac{1}{N_a} \sum_{j=1}^{N_a} |\phi_j\rangle \langle \phi_j|,$$

where  $|\phi_j\rangle = |g_1, \dots, g_{j-1}, r_j, g_{j+1}, \dots, g_{N_a}\rangle$ .

The basis states of the combined atomic-molecular system are  $|\Psi_{\text{atom}}\rangle |\Psi_{\text{mol}}\rangle$ , where  $|\Psi_{\text{mol}}\rangle = |a_1 \dots a_N\rangle$  and  $|a_i\rangle = |J, m_J\rangle_i$ . Matrix elements of the Hamiltonian of the system

$$H = H_a + H_m + V_{e^- - M} \quad (5)$$

with  $H_a = \sum_{j=1}^{N_a} E_{r_j} |r_j\rangle \langle r_j|$ ,  $H_m = \sum_{i=1}^N B J_i^2$  and  $V_{e^- - M} = \sum_{j=1}^{N_a} \sum_{i=1}^N \frac{e\vec{d}_i \cdot \vec{R}_{ji}}{R_{ji}^3} - \frac{e\vec{d}_i \cdot (\vec{R}_{ji} - \vec{r})}{|\vec{R}_{ji} - \vec{r}|^3}$ , have the form

$$\begin{aligned} \langle \Psi_{\text{atom}} | \langle \Psi_{\text{mol}} | H_a | \Phi_{\text{mol}} \rangle | \Psi_{\text{atom}} \rangle &= \\ &= -\frac{1}{2(n_s - \mu_s)^2} \Pi_{i=1}^N \delta_{a_i, a'_i}, \end{aligned} \quad (6)$$

$$\begin{aligned} \langle \Psi_{\text{atom}} | \langle \Psi_{\text{mol}} | H_m | \Phi_{\text{mol}} \rangle | \Psi_{\text{atom}} \rangle &= \\ &= \left( \sum_{i=1}^N B J_i (J_i + 1) \right) \Pi_{i=1}^N \delta_{a_i, a'_i}, \end{aligned}$$

$$\begin{aligned} \langle \Psi_{\text{atom}} | \langle \Psi_{\text{mol}} | V_{e^- - M} | \Phi_{\text{mol}} \rangle | \Psi_{\text{atom}} \rangle &= \\ &= \left( \frac{1}{N_a} \sum_{j=1}^{N_a} \langle a_i | V_{ji} | a'_i \rangle \right) \Pi_{k=1, k \neq i}^N \delta_{a_k, a'_k} \delta_{J_i, J'_i \pm 1}, \end{aligned}$$

for  $i = 1 \dots N$ , where  $|\Phi_{\text{mol}}\rangle = |a'_1, a'_2, \dots, a'_i, \dots, a'_N\rangle$ .

For a simplified analysis we also take into account only  $|J = 0, m_J = 0\rangle$  and  $|J = 1, m_J = 0\rangle$  rotational states in

diagonalizing the Hamiltonian. Using only  $J = 0$  and  $J = 1$  states makes calculations of the matrix elements  $\langle a_i | V_{ji} | a'_i \rangle$  particularly simple. For the atom located next to the molecules at  $\Delta x = 0$  the matrix elements are calculated as described in part (2) of App. A. For an atom separated from the molecule by a lattice spacing(s) the matrix elements can be calculated as discussed in part (3) of App. A.

If the interaction strength is much smaller than the rotational splitting between the  $J = 0$  and  $J = 1$  states  $|V_{e^- - M}| \ll E_{\text{rot}}$ , where  $E_{\text{rot}} = 2B$ , and only the  $ns$  state is taken into account, the shifted energies of the collective rotational states can be calculated using second-order perturbation theory. All unperturbed states  $(k \uparrow, (N - k) \downarrow)$  with  $k$  spins up and  $N - k$  spins down have the same energy  $E_{(k \uparrow, (N - k) \downarrow)} = kE_{\text{rot}}$ , and groups of states differing by one flipped spin are separated by the rotational splitting  $E_{\text{rot}}$ . The interaction weakly couples states in neighboring spin groups resulting in shifts of their energy. Let us consider first the  $|ns\rangle |\downarrow, \downarrow, \dots, \downarrow\rangle$  state for  $N$  molecules and  $N_a$  atoms. The energy shift of this state will be given by:

$$\begin{aligned} \Delta E_{N\downarrow} &= \\ &= - \sum_{i=1}^N \frac{|\langle \Psi_{\text{atom}} | \langle \downarrow, \dots, \downarrow | V_{e^- - M} | \downarrow, \dots, \uparrow_i, \dots, \downarrow \rangle | \Psi_{\text{atom}} \rangle|^2}{E_{\text{rot}}} = \\ &= - \sum_{i=1}^N \frac{|\langle \downarrow_i | \sum_{j=1}^{N_a} \langle ns_j | V_{e^- - M} | ns_j \rangle / N_a | \uparrow_i \rangle|^2}{E_{\text{rot}}} = \\ &= - \sum_{i=1}^N \frac{|\sum_{j=1}^{N_a} V_{e^- - M}^{ji}|^2}{E_{\text{rot}} N_a^2}. \end{aligned}$$


---

Assuming for simplicity that  $i^{\text{th}}$  molecule most strongly interacts with its nearest atom with  $j = i$  and the matrix elements  $V_{e^- - M}^{j=i}$  are the same for all  $i$ , the shift can be approximated as

$$\Delta E_{N\downarrow} \approx - \frac{\sum_{i=1}^N |V_{e^- - M}^{j=i}|^2}{E_{\text{rot}} N_a^2} \approx - \frac{N |V_{e^- - M}^{j=i}|^2}{E_{\text{rot}} N_a^2},$$

which gives the dependence  $\Delta E_{N\downarrow} \sim 1/N$  for  $N_a \sim N$ . For states with a single  $i^{\text{th}}$  spin up and  $i' = 1, \dots, i - 1, i + 1, \dots, N$  spins down, the perturbation theory gives the energy shift

$$\begin{aligned} \Delta E_{(1\uparrow, (N-1)\downarrow)} &= - \sum_{i'=1, i' \neq i}^N \frac{|\langle \Psi_{\text{atom}} | \langle \downarrow, \dots, \uparrow_i, \dots, \downarrow | V_{e^- - M} | \downarrow, \dots, \uparrow_i, \dots, \uparrow_{i'}, \dots, \downarrow \rangle | \Psi_{\text{atom}} \rangle|^2}{E_{\text{rot}}} + \\ &+ \frac{|\langle \Psi_{\text{atom}} | \langle \downarrow, \dots, \uparrow_i, \dots, \downarrow | V_{e^- - M} | \downarrow, \dots, \downarrow \rangle | \Psi_{\text{atom}} \rangle|^2}{E_{\text{rot}}} = \\ &= - \frac{1}{N_a^2} \sum_{i'=1, i' \neq i}^N \frac{|\sum_{j=1}^{N_a} V_{e^- - M}^{ji'}|^2}{E_{\text{rot}}} + \frac{1}{N_a^2} \frac{|\sum_{j=1}^{N_a} V_{e^- - M}^{ji}|^2}{E_{\text{rot}}} \approx - \frac{(N-1) |V_{e^- - M}^{j=i'}|^2}{N_a^2 E_{\text{rot}}} + \frac{1}{N_a^2} \frac{|V_{e^- - M}^{j=i}|^2}{E_{\text{rot}}} = \\ &= - \frac{(N-2) |V_{e^- - M}^{j=i}|^2}{N_a^2 E_{\text{rot}}}, \end{aligned}$$


---

which shows that the splitting between the  $N \downarrow$  and  $(1 \uparrow, (N - 1) \downarrow)$  states  $\sim 2|V_{e^- - M}|^2 / E_{\text{rot}} N_a^2 \sim 1/N^2$ . In the

general case of  $(k \uparrow, (N - k) \downarrow)$  states the shift will be given by

$$\begin{aligned}
\Delta E_{(k\uparrow, (N-k)\downarrow)} &= -\frac{1}{N_a^2} \sum_{i'=1, i' \in (N-k)\downarrow}^N \frac{|\sum_{j=1}^{N_a} V_{e^- - M}^{ji'}|^2}{E_{\text{rot}}} + \frac{1}{N_a^2} \sum_{i=1, i \in k\uparrow}^N \frac{|\sum_{j=1}^{N_a} V_{e^- - M}^{ji}|^2}{E_{\text{rot}}} \approx \\
&\approx -\frac{(N-k) |V_{e^- - M}^{j=i'}|^2}{N_a^2 E_{\text{rot}}} + \frac{k |V_{e^- - M}^{j=i}|^2}{N_a^2 E_{\text{rot}}} \approx -\frac{(N-2k) |V_{e^- - M}^{j=i}|^2}{N_a^2 E_{\text{rot}}}.
\end{aligned} \tag{7}$$

The energies of the collective states will also get an additional contribution  $\sim \Delta E_{(k\uparrow, (N-k)\downarrow)}(2a^2/\rho^2)$  due to a finite spread of atomic and molecular positions in their traps, as shown in App. C.

In the case when only the  $ns$  atomic state is taken into account there will be no terms exchanging spins within the same group such as e.g.  $|\downarrow, \cdot, \uparrow_i, \cdot, \downarrow_{i'}, \cdot, \downarrow\rangle \leftrightarrow |\downarrow, \cdot, \downarrow_i, \cdot, \uparrow_{i'}, \cdot, \downarrow\rangle$  in the  $(1 \uparrow, (N-1) \downarrow)$  manifold. The spin-exchange terms will be absent because the second-order perturbation theory connects these states via a single state in the upper and a single state in the lower neighboring spin groups, which cancel each other due to the equal splitting between neighbouring groups. There will be spin-exchange terms within the groups due to a direct dipole-dipole interaction between molecules, which has not been taken into account in the Hamiltonian (5). The direct dipole-dipole interaction allows spin-exchange processes within the same group leading to splittings  $\sim d^2/L^3 \sim 1$  kHz for  $d \sim 1$  D and a lattice period  $L \sim 500$  nm, which is of the order of the width of the 60s state.

In the following we numerically consider a system of  $N = 3$  and 5 KRb and RbYb molecules interacting with a Rb superatom. Due to the small size of the considered molecular arrays, if one uses an atomic array of the same size, effects of the boundaries will be sizable, because the molecules in the center will strongly interact with all three nearest atoms, while the molecules at the boundaries will interact strongly with only two atoms. This is not going to be the case in a sufficiently long array, in which all molecules (again, except for two boundary ones) will have equal interaction conditions. To mitigate the effects of the boundaries we therefore consider an array of  $N_a = N + 2$  atoms, arranged in a way shown in Fig. 3a such that there is an additional atom at each side of the molecular array. In this arrangement all molecules will interact strongly with three nearest atoms, i.e. separated by at most one lattice period  $L = 500$  nm. Atoms separated from a molecule by two or more lattice periods do not contribute significantly for the 60s Rydberg state.

Energy shifts of the states of a combined atomic-molecular system from the unperturbed values  $E_{(k\uparrow, (N-k)\downarrow)}$ , corresponding to different collective rotational states, are given in Fig. 4 for KRb and RbYb in the left and right columns, respectively. Since only the 60s Rydberg state and  $J = 0$  and  $J = 1$  rotational states have been used in calculation of matrix elements of the Hamiltonian Eq. (5), the magnitude of the shifts is

only qualitatively correct. In order to get quantitatively correct shifts the closest in energy p, d and f Rydberg states as well as  $J = 2$  rotational states have to be taken into account, which is beyond the scope of our work. Fig. 4 shows the shifts calculated by (i) diagonalization of the Hamiltonian Eq. (5) and (ii) using perturbation theory expression (7) with  $V_{e^- - M}^{ji}$  calculated numerically. The results of the two calculations agree very well.

From Fig. 4 one can see that the states with the same number of spins up and down such as  $|\uparrow, \downarrow, \downarrow\rangle$ ,  $|\downarrow, \uparrow, \downarrow\rangle$  and  $|\downarrow, \downarrow, \uparrow\rangle$  group, as expected, so only states with at least one spin flipped significantly differ in energy and can be discerned. For  $N = 3$  the spin groups split from each other by  $\sim 150 - 50$  kHz for  $300 \text{ nm} < \rho < 500 \text{ nm}$  for KRb and by  $\sim 600 - 200$  kHz for  $400 \text{ nm} < \rho < 600 \text{ nm}$  for RbYb. For an array of  $N = 5$  molecules, shown in Fig. 4c and d, the energy splittings between spin groups become smaller:  $\sim 70 - 10$  kHz for KRb, and  $\sim 300 - 100$  kHz for RbYb in the same ranges of  $\rho$ . The reduction of the splittings with increasing  $N$  comes from the simultaneous increase in  $N_a$  as expected from Eq. (7). It suggests that for larger  $N$  the splittings will get even smaller and eventually become comparable to the width of the Rydberg state. The states will no longer be discernable and there will be a continuous band of collective molecular states.

In experiments it can be difficult to have two parallel optical lattices, one filled with molecules and another with atoms. The setup will be simplified if the atoms are placed in a cigar-shaped dipole trap with a long axis parallel to the molecular array as shown in Fig. 3b. We modelled the interaction of a molecular array with a Rydberg superatom placed in such a trap by assuming that the excited atom has a Gaussian 1D probability distribution  $p(x) = \exp(-x^2/a_{\text{trap}}^2)/a_{\text{trap}}\sqrt{\pi}$  along the longest trap axis with  $x = 0$  corresponding to the center of the molecular array. In this case the summation  $\sum_{j=1}^{N_a} V_{ji}/N_a$  over atom's  $j$  position in Eqs. (4) and (6) is replaced by an integral  $\int V_i(x)p(x)dx$ . Fig. 5a(c) and b(d) show the shifts of the collective states for  $N = 3$ (5) for KRb and RbYb, respectively, obtained by diagonalization of (5). The size of the atomic distribution  $a_{\text{trap}}$  was chosen to have the largest splittings between spin states differing by one flipped spin. Compared to the case of atoms in a lattice the shifts between spin groups become about twice smaller for  $N = 3$  and three times smaller for  $N = 5$  for both KRb and RbYb. The splittings within groups ap-

pear, and for  $N = 5$  become comparable to the splittings between the groups. The reason for splittings within the groups is in the unequal interaction conditions for molecules in the center and at the boundaries. Due to the decrease of the atom's probability from the center to the edges of the trap the corresponding molecules will experience weaker interaction. The interaction conditions can be made more homogeneous if the trap size in the longitudinal direction is much larger than the molecular array's, but in this case the probability to find the atom in the range  $(X_i - L/2, X_i + L/2)$  around  $i^{\text{th}}$  molecule position  $X_i$  will be smaller than the corresponding probability  $1/N_a$  of atoms in a lattice.

The  $\sim 1/N$  and  $\sim 1/N^2$  scalings of the spin group energy shifts and splittings can be avoided if the molecules are placed in a ring 1D array [44] instead of a linear one. In this case if the superatom (or a single Rydberg atom) is placed at the center of the array and its size is much smaller than the radius of the array all interaction matrix elements  $V_{e^-M}^{ji}$  will be equal for a symmetric  $ns$  state  $V_{e^-M}^{ji} = \tilde{V}_{e^-M}$  and the shifts (7) will become:

$$\begin{aligned} \Delta E_{(k\uparrow, (N-k)\downarrow)} &= -(N-k) \frac{|\tilde{V}_{e^-M}|^2}{E_{\text{rot}}} + k \frac{|\tilde{V}_{e^-M}|^2}{E_{\text{rot}}} \approx \\ &\approx -(N-2k) \frac{|\tilde{V}_{e^-M}|^2}{E_{\text{rot}}}, \end{aligned}$$

which shows that in this case the shifts and splittings scale as  $\Delta E \sim N|\tilde{V}_{e^-M}|^2/E_{\text{rot}}$  and  $\sim 2|\tilde{V}_{e^-M}|^2/E_{\text{rot}}$  with the number of the molecules, so the splittings are limited by the interaction strengths  $|\tilde{V}_{e^-M}|^2$ , falling with the atom-molecule distance, equal to the radius of the array, as  $1/R_{ji}^4$ .

Selective excitation to the Rydberg state for a particular spin group will require the Rabi frequency  $\Omega$  of an exciting optical pulse be smaller than the splittings between spin groups. With the splittings between spin groups  $\sim$  hundreds kHz one can use  $\Omega = 10$  kHz. In this case the blockade radius for the  $60s$  state will be of the order of  $R_b = (C_6/\hbar\Omega)^{1/6} \sim 2.2 \mu\text{m}$ , where  $C_6$  is taken from [45]. For the linear array period  $L = 500$  nm the blockade can be realized for  $N_a \leq 9$  atoms in  $60s$ , i.e. higher  $n$  are required for larger arrays. For example, for  $n = 100$  and the same Rabi frequency  $\Omega = 10$  kHz the blockade radius will be  $\approx 44 \mu\text{m}$ , which will allow to use a linear array of  $\sim 200$  atoms and molecules. In a ring array any number of atoms can be used provided the atomic trap size is smaller than the blockade radius.

## V. MEASUREMENT OF ROTATIONAL STATE POPULATION

Let us first discuss the measurement of rotational states population of a single molecule interacting with a single Rydberg atom. In this case we assume that each molecule in an array or optical lattice has its own readout atom, which can be addressed individually using tightly

focussed laser beams and excited to the Rydberg state without affecting neighboring atoms. Individual addressing of atoms in an optical lattice with a lattice period  $\lambda/2 \sim 500$  nm has been demonstrated recently in [47]. Alternatively, low cross-talk addressing of atoms can be realized if, before the readout, the molecular and atomic lattices period is increased to values  $\sim$  several  $\mu\text{m}$  using tunable-period 1D or 2D optical lattices [48].

The populations of the ground and first excited rotational states can be read out in the following way (see Fig. 6a). First, the atom is prepared in the ground state, e.g.  $|g\rangle = |F = 2, m_F = 2\rangle$  for Rb, such that the state of the combined system is  $(\alpha|\downarrow\rangle + \beta|\uparrow\rangle)|g\rangle$ , where  $|\alpha|^2$  and  $|\beta|^2$  are the molecular qubit states populations to be read out. The combined system next is transferred selectively from e.g. the  $|g\rangle|\uparrow\rangle$  to the  $|r\rangle|\uparrow\rangle$ , where  $|r\rangle$  is the atomic Rydberg state, with a  $\pi$  pulse, followed by another  $\pi$  pulse transferring the system from the  $|r\rangle|\uparrow\rangle$  to some axially  $|e\rangle|\uparrow\rangle$  state with a short lifetime, which rapidly decays back to  $|g\rangle|\uparrow\rangle$  [49]. Repeating the excitation-fluorescence cycle one can detect the population  $|\beta|^2$  of the  $|\uparrow\rangle$  rotational state. Another way to read out populations of molecular qubits is shown in Fig. 6b,c and d. While the atom is in the ground state its fluorescence is measured using the cycling transition  $|g\rangle \rightarrow |e\rangle$ , which will include contributions from both rotational states with probabilities  $|\alpha|^2$  and  $|\beta|^2$  (Fig. 6b). Next a  $\pi$  optical pulse is applied to excite the system conditionally only if the molecule is in the  $|\uparrow\rangle$  state, producing an entangled state of the combined system  $\alpha|\downarrow\rangle|g\rangle + \beta|\uparrow\rangle|r\rangle$ , and again the atomic fluorescence is measured using the cycling transition (Fig. 6c). This time the part of the atom in the Rydberg state will not fluoresce and only the  $|g\rangle|\downarrow\rangle$  part will contribute with the probability  $|\alpha|^2$  (Fig. 6d). By measuring the ratio of fluorescence intensities in the two cases  $R = |\alpha|^2/(|\alpha|^2 + |\beta|^2)$  one can calculate the populations of the rotational states  $|\alpha|^2 = R$  and  $|\beta|^2 = 1 - R$ . The Rydberg state has a finite lifetime and can decay during the readout steps of Fig. 6c,d. The decay can be avoided if the atom is transferred to a stable ground state  $|g'\rangle$  by a  $\pi$  pulse:  $|g\rangle|\uparrow\rangle \rightarrow |r\rangle|\uparrow\rangle \rightarrow |g'\rangle|\uparrow\rangle$  such that  $|g'\rangle$  is not affected by the excitation-fluorescence cycles  $|g\rangle \leftrightarrow |e\rangle$ . Additionally, it allows one to entangle two atomic ground states and two rotational molecular states as  $(\alpha|\downarrow\rangle + \beta|\uparrow\rangle)|g\rangle \rightarrow \alpha|g\rangle|\downarrow\rangle + \beta|g'\rangle|\uparrow\rangle$ . The  $\pi$  pulses can be replaced by coherent control pulse sequences such as STIRAP or ARP (adiabatic rapid passage), more robust with respect to pulse duration and intensity fluctuations.

As was discussed in Section III the energies of the  $|r\rangle|\downarrow\rangle$ ,  $|r\rangle|\uparrow\rangle$  states are additionally shifted due to a finite spread of atomic and molecular positions in their traps. This additional shift might tune the Rydberg state out of resonance with an excitation laser. This difficulty can be overcome by using the Rabi frequency of the excitation pulses large enough to cover the additional shift, but small enough to provide selective excitation to a particular rotational state. As shown in App. D the additional

shifts of the  $|J = 0, m_J = 0\rangle$  and  $|J = 1, m_J = 0\rangle$  states are of the order of  $\leq 20$  kHz for KRb and  $\leq 40$  kHz for RbYb, and for the  $|J = 1, m_J = \pm 1\rangle$  states they are of the order of  $\leq 60$  kHz for KRb and  $\leq 7$  kHz for RbYb. Given the splittings between the states  $\sim 1$  MHz for KRb and  $\sim 3$  MHz for RbYb the Rabi frequency satisfying both requirements can be realized. Another solution is to excite the atom using ARP with a chirped pulse such that the frequency sweep covers the additional energy shift.

The main part of the measurement described in Fig. 6 is a CNOT gate applied to the atom-molecule system. The measurement based on the CNOT gate is of a quantum non-demolition type, in which the measurement is done on the ancilla system after it has interacted with the primary system in such a way that the primary system is not destroyed and its projected states are not disturbed by the measurement [50]. In [51] requirements for a QND measurement on a primary qubit by an ancilla qubit have been derived in terms of fidelities of measurement  $F_M = \sqrt{\sum_i p_i^M p_i^{\text{in}}}$ , QND fidelity  $F_{\text{QND}} = \sqrt{\sum_i p_i^{\text{in}} p_i^{\text{out}}}$  and the quantum state preparation fidelity  $F_{\text{QSP}} = \sum_i p_i^M p_{|i\rangle}^{\text{out}}$ , where  $p_i^{\text{in}}$ ,  $p_i^M$  and  $p_i^{\text{out}}$  are the probability distributions of the input, measured and output states in the basis of the eigenstates  $|i\rangle$  of the measurement;  $p_{|i\rangle}^{\text{out}}$  is the conditional probability of finding the output state to be  $|i\rangle$  if the measurement gave the eigenvalue  $i$ . The CNOT gate gives  $F_M = F_{\text{QND}} = F_{\text{QSP}} = 1$ , i.e. it represents an ideal QND measurement. The QND nature of the measurement can be seen from the form of the actual atom-molecule interaction

$$\begin{aligned} |ns\rangle \langle ns| (\Delta E_\uparrow |\uparrow\rangle \langle \uparrow| + \Delta E_\downarrow |\downarrow\rangle \langle \downarrow|) &= \\ &= \left( \hat{S}_z^{\text{at}} + \frac{1}{2} \right) \left( \Delta E_\uparrow (\hat{S}_z^{\text{mol}} + \frac{1}{2}) + \Delta E_\downarrow (\frac{1}{2} - \hat{S}_z^{\text{mol}}) \right) \\ &= (\Delta E_\uparrow - \Delta E_\downarrow) \hat{S}_z^{\text{at}} \hat{S}_z^{\text{mol}} + \hat{S}_z^{\text{at}} \frac{\Delta E_\downarrow + \Delta E_\uparrow}{2} + \\ &\quad + \hat{S}_z^{\text{mol}} \frac{\Delta E_\downarrow - \Delta E_\uparrow}{2}, \end{aligned}$$

which commutes with the measured observable  $\hat{S}_z^{\text{mol}}$ . Here  $\hat{S}_z^{\text{at}} = (|ns\rangle \langle ns| - |g\rangle \langle g|)/2$  and  $\hat{S}_z^{\text{mol}} = (|\uparrow\rangle \langle \uparrow| - |\downarrow\rangle \langle \downarrow|)/2$ .

The QND measurement based on the CNOT gate has been used previously in systems of two ions [52], electron-nuclear spins of N-V center [53] and was also theoretically discussed for a system of two neutral atoms of different species, interacting in Rydberg states [54].

Finally, we come to the main point of the work and discuss how population of collective rotational states can be measured in a molecular array interacting with a Rydberg superatom. The measurement is based on the interaction induced splittings between spin groups  $|k \uparrow, (N-k) \downarrow\rangle$  for  $k = 0, \dots, N$ , analyzed in the previous section. As shown in Fig. 7, first, the com-

bined system is excited selectively from some group of  $k \uparrow$  spins up  $|g, g, \dots, g\rangle |\Psi_{\text{mol } k \uparrow}\rangle$  to the blocked state  $|\Psi_{\text{atom}}\rangle |\Psi_{\text{mol } k \uparrow}\rangle$  by a  $\pi$  pulse, followed by another  $\pi$  pulse connecting the  $|\Psi_{\text{atom}}\rangle$  state to some  $|\Psi_e\rangle = \frac{1}{\sqrt{N_a}} \sum_{j=1}^{N_a} e^{i(k_x \text{Rydb} - k_x e) X_j} |g_1, g_2, \dots, e_j, \dots, g_{N_a}\rangle$  state, where  $|e\rangle$  is an atomic state rapidly decaying to  $|g\rangle$ . Again, instead of two  $\pi$  pulses a sequence of either STIRAP or ARP pulses can be used. The collective states will also acquire an additional energy shift due to a finite spread of atomic and molecular positions in their traps, which should be taken into account when exciting the atom to the Rydberg state. It can be done either using a sufficiently large Rabi frequency of the excitation pulse, or using a chirped pulse. By repeating these excitation-fluorescence cycles the population of the  $|\Psi_{\text{mol } k \uparrow}\rangle$  can be detected. Let us illustrate the scheme for  $N = 3$  molecules. Initially, the molecular system is in a superposition of all spin states:

$$\begin{aligned} |\Psi_{\text{mol}}\rangle &= a_{\downarrow, \downarrow, \downarrow} |\downarrow, \downarrow, \downarrow\rangle + a_{\uparrow, \downarrow, \downarrow} |\uparrow, \downarrow, \downarrow\rangle + \\ &\quad + a_{\downarrow, \uparrow, \downarrow} |\downarrow, \uparrow, \downarrow\rangle + a_{\downarrow, \downarrow, \uparrow} |\downarrow, \downarrow, \uparrow\rangle + \\ &\quad + a_{\uparrow, \uparrow, \downarrow} |\uparrow, \uparrow, \downarrow\rangle + a_{\uparrow, \downarrow, \uparrow} |\uparrow, \downarrow, \uparrow\rangle + \\ &\quad + a_{\downarrow, \uparrow, \uparrow} |\downarrow, \uparrow, \uparrow\rangle + a_{\uparrow, \uparrow, \uparrow} |\uparrow, \uparrow, \uparrow\rangle. \end{aligned}$$

Suppose one is to measure the total population of the states with one spin up and two spins down, i.e. the  $|\uparrow, \downarrow, \downarrow\rangle, |\downarrow, \uparrow, \downarrow\rangle, |\downarrow, \downarrow, \uparrow\rangle$  states. For that the initial state  $|g, g, \dots, g\rangle |\Psi_{\text{mol}}\rangle$  is transformed into

$$\begin{aligned} |g, g, \dots, g\rangle &(a_{\downarrow, \downarrow, \downarrow} |\downarrow, \downarrow, \downarrow\rangle + a_{\uparrow, \uparrow, \downarrow} |\uparrow, \uparrow, \downarrow\rangle + \\ &\quad + a_{\uparrow, \downarrow, \uparrow} |\uparrow, \downarrow, \uparrow\rangle + a_{\downarrow, \uparrow, \uparrow} |\downarrow, \uparrow, \uparrow\rangle + \\ &\quad + a_{\uparrow, \uparrow, \uparrow} |\uparrow, \uparrow, \uparrow\rangle) + |\Psi_{\text{atom}}\rangle (a_{\uparrow, \downarrow, \downarrow} |\uparrow, \downarrow, \downarrow\rangle + \\ &\quad + a_{\downarrow, \uparrow, \downarrow} |\downarrow, \uparrow, \downarrow\rangle + a_{\downarrow, \downarrow, \uparrow} |\downarrow, \downarrow, \uparrow\rangle) = \\ &= |g, g, \dots, g\rangle (|\Psi_{\text{mol}}\rangle - |\Psi_{\text{mol } k \uparrow=1}\rangle) + |\Psi_{\text{atom}}\rangle |\Psi_{\text{mol } k \uparrow=1}\rangle, \end{aligned}$$

by selective excitation to the Rydberg superatom state, where we denote the part of the state corresponding to a single spin up as

$$|\Psi_{\text{mol } k \uparrow=1}\rangle = a_{\uparrow, \downarrow, \downarrow} |\uparrow, \downarrow, \downarrow\rangle + a_{\downarrow, \uparrow, \downarrow} |\downarrow, \uparrow, \downarrow\rangle + a_{\downarrow, \downarrow, \uparrow} |\downarrow, \downarrow, \uparrow\rangle.$$

Next, atoms in  $|\Psi_{\text{atom}}\rangle$  are transferred to the state  $|\Psi_e\rangle$ , which rapidly decays to the  $|g, g, \dots, g\rangle$  state. Repeating the excitation-fluorescence cycles and detecting fluorescence intensity will allow one to obtain the total population of the  $|\Psi_{\text{mol } k \uparrow=1}\rangle$  state, given by  $|a_{\uparrow, \downarrow, \downarrow}|^2 + |a_{\downarrow, \uparrow, \downarrow}|^2 + |a_{\downarrow, \downarrow, \uparrow}|^2$ . Applying this sequence for all  $|\Psi_{\text{mol } k \uparrow}\rangle$ , populations of all spin groups can be measured. This measurement is non-destructive with respect to molecules and is also of a QND type and will in fact project the molecular system to a superposition of states with a certain number of spins up and down provided a spontaneously emitted photon is detected. In this way entangled many-body molecular states can be prepared by measurement, which does not require molecules to interact, similar to the proposals in cQED systems [55]. For example, if initially all molecules are prepared in an equal superposition

state  $(|\downarrow\rangle_i + |\uparrow\rangle_i)/\sqrt{2}$ , and the described above measurement sequence is applied, one will be able to project the system to an entangled state, which is an equal superposition of states with one spin up - W state, and more generally, equal superpositions of states with  $k$  spins up and  $N-k$  spins down - Dicke states. The collective states readout scheme could also be applied to measure the estimated Hamming weight of the molecular spin string  $N_{\text{est}} = \sum k \uparrow p_{k\uparrow}$ , where  $0 \leq k \uparrow \leq N$  is the number of spins up in a particular spin group and  $p_{k\uparrow}$  is the probability of such a group, measured in our case by atomic fluorescence intensity. The Hamming weight, which is the total number of spins up in a string of  $N$  spins or qubits, is a useful quantity in quantum error correction [56] and in ion string clocks for determining the deviation of the clock frequency from an unperturbed ion frequency [57].

## VI. CONCLUSION

We present a detailed analysis for non-destructive readout of mesoscopic ensembles of polar molecules, by exploiting the exquisite sensitivity of Rydberg states in interaction with molecular rotational states. The extreme dipole moment of the Rydberg atoms allows selective addressing of single or collective molecular rotational states. Our earlier proposal dealt only with single atoms and single molecules and found that, for example for distances of 300 - 600 nm between molecule and atom a shift of several MHz can be detected in the Rydberg level depending on the molecular rotational state. This is wider than any line widths in this setup.

In the present article, we have shown that these shifts, and the ensuing possibility of conditional Rydberg excitation and thus atom-molecule entanglement allows non-demolition readout not only for single atom-molecule pairs but also for collective rotational states in molecular ensembles. In the latter case instead of a single atom a Rydberg superatom, i.e., a single Rydberg excitation of a small ensemble of atoms, can be used.

In particular, detailed numerical estimates for small arrays of ground state KRb or RbYb molecules show that the difference of one excited collective rotational state leads to shifts of 100s of kHz in a Rydberg superatom about half a  $\mu\text{m}$  away. Our calculations were done for atoms in both a linear array and a dipole trap, often an easier experimental setup. Calculations in this case

predict only a slightly smaller shift, which shows that the regularity in an optical lattice is not the defining feature of the setup.

While, at the present status of experiments, arrays of different species of under a  $\mu\text{m}$  distance might still be challenging (although two close lattices were demonstrated for the same atomic species [23]), the techniques presented here address particularly the non-destructive readout of single or collective molecular rotational states, which has been a mostly unsolved problem to date. With the size of the Rydberg shifts of hundreds kHz, the superatom can be conditionally excited depending on the collective molecular state. While the fluorescence of the atom(s) is measured, effectively reading out the molecular state, the molecules remain untouched. An obvious extension would be to use the Rydberg atom(s) as a communication channel between two molecules or two molecular ensembles, thus allowing for effective indirect interactions between the molecular dipoles that are much stronger than the direct dipole-dipole interaction between the molecules. Proposals for many-body states based on strongly interacting dipoles could potentially be realized much easier this way. In addition, the conditional excitation allows very well controlled entanglement between molecules or groups of molecules, thus opening the door to, for example, entanglement-enhanced metrology.

## VII. ACKNOWLEDGEMENTS

E.K. was supported by the Russian Science Foundation (grant 16-12-00028) in the part of analysis of rotational states readout via atom-molecule entanglement, and the Russian Fund for Basic Research (grants RFBR 14-02-00174), and would like to thank the Institute for Theoretical Atomic and Molecular Physics for hospitality and financial support during her visit. SFY would like to thank the NSF for funding. S.T.R. acknowledges support from NSF Grants No. PHY-1516337 and No. PHY-1516421 and from a Cottrell College Science Award through the Research Corporation for Scientific Advancement.

## Appendix A

### 1. Calculation of interaction matrix elements Eq. (2) in a general case

In order to calculate the matrix elements of the interaction term  $(V_{e-M})_{nlmJm_J,n'l'm'_Jm'_J} = \langle J, m_J | e\vec{d} | J', m'_J \rangle \langle n l m | \frac{\vec{R}}{R^3} | n' l' m' \rangle - \langle J, m_J | e\vec{d} | J', m'_J \rangle \langle n l m | \frac{\vec{R}-\vec{r}}{|\vec{R}-\vec{r}|^3} | n' l' m' \rangle$  we assume that the Rydberg atom is fixed at its position by e.g. trapping in a deep dipole trap or optical lattice such that  $\vec{R} = R_x \vec{e}_x + R_y \vec{e}_y + R_z \vec{e}_z$ .

The molecular dipole moment can be written as  $\vec{d} = d_x \vec{e}_x + d_y \vec{e}_y + d_z \vec{e}_z$  leading to:

$$\vec{d}(\vec{R} - \vec{r}) = d_x(R_x - r \sin \theta \cos \phi) + d_y(R_y - r \sin \theta \sin \phi) + d_z(R_z - r \cos \theta),$$

where  $\theta$  and  $\phi$  are the polar and azimuthal angles of the electron with respect to the Rydberg core.

As a result,

$$V_{e^- - M} = \frac{e(d_x R_x + d_y R_y + d_z R_z)}{R^3} - \frac{ed_x(R_x - r \sin \theta \cos \phi) + ed_y(R_y - r \sin \theta \sin \phi) + ed_z(R_z - r \cos \theta)}{((R_x - r \sin \theta \cos \phi)^2 + (R_y - r \sin \theta \sin \phi)^2 + (R_z - r \cos \theta)^2)^{3/2}},$$

which can be written as  $V_{e^- - M} = V_{e^- - M}^{\text{core}} + V_{e^- - M}^{\text{el}}$  with

$$\begin{aligned} V_{e^- - M}^{\text{core}} &= \frac{e(d_x R_x + d_y R_y + d_z R_z)}{R^3}, \\ V_{e^- - M}^{\text{el}} &= -\frac{ed_x(R_x - r \sin \theta \cos \phi) + ed_y(R_y - r \sin \theta \sin \phi) + ed_z(R_z - r \cos \theta)}{((R_x - r \sin \theta \cos \phi)^2 + (R_y - r \sin \theta \sin \phi)^2 + (R_z - r \cos \theta)^2)^{3/2}} = \\ &= ed_x \frac{\partial}{\partial R_x} \frac{1}{((R_x - r \sin \theta \cos \phi)^2 + (R_y - r \sin \theta \sin \phi)^2 + (R_z - r \cos \theta)^2)^{1/2}} + \\ &+ ed_y \frac{\partial}{\partial R_y} \frac{1}{((R_x - r \sin \theta \cos \phi)^2 + (R_y - r \sin \theta \sin \phi)^2 + (R_z - r \cos \theta)^2)^{1/2}} + \\ &+ ed_z \frac{\partial}{\partial R_z} \frac{1}{((R_x - r \sin \theta \cos \phi)^2 + (R_y - r \sin \theta \sin \phi)^2 + (R_z - r \cos \theta)^2)^{1/2}}. \end{aligned}$$

Let us express the vector connecting the core and the molecule via its spherical coordinates (see Fig. 8)  $\vec{R} = (R \sin \eta \cos \nu, R \sin \eta \sin \nu, R \cos \eta)$  and express the derivatives  $\frac{\partial}{\partial R_x}$ ,  $\frac{\partial}{\partial R_y}$ ,  $\frac{\partial}{\partial R_z}$  via spherical coordinates as well:

$$\begin{aligned} \frac{\partial}{\partial R_x} &= \sin \eta \cos \nu \frac{\partial}{\partial R} + \frac{\cos \eta \cos \nu}{R} \frac{\partial}{\partial \eta} - \frac{\sin \nu}{R \sin \eta} \frac{\partial}{\partial \nu}, \\ \frac{\partial}{\partial R_y} &= \sin \eta \sin \nu \frac{\partial}{\partial R} + \frac{\cos \eta \sin \nu}{R} \frac{\partial}{\partial \eta} + \frac{\cos \nu}{R \cos \eta} \frac{\partial}{\partial \nu}, \\ \frac{\partial}{\partial R_z} &= \cos \eta \frac{\partial}{\partial R} - \frac{\sin \eta}{R} \frac{\partial}{\partial \eta}. \end{aligned}$$

Next we can use the expansion

$$\begin{aligned} \frac{1}{\sqrt{R^2 + r^2 - 2rR \cos \gamma}} &= 4\pi \sum_{l''=0}^{\infty} \frac{1}{2l''+1} \frac{r_{<}^{l''}}{r_{>}^{l''+1}} \sum_{m''=-l''}^{m''=l''} Y_{l''}^{m''}(\theta, \phi) Y_{l''}^{m''*}(\eta, \nu) = \\ &= 4\pi \begin{cases} \sum_{l''=0}^{\infty} \frac{1}{2l''+1} \frac{r^{l''}}{R^{l''+1}} \sum_{m''=-l''}^{l''} Y_{l''}^{m''}(\theta, \phi) Y_{l''}^{m''*}(\eta, \nu) & \text{for } r < R \\ \sum_{l''=0}^{\infty} \frac{1}{2l''+1} \frac{R^{l''}}{r^{l''+1}} \sum_{m''=-l''}^{l''} Y_{l''}^{m''}(\theta, \phi) Y_{l''}^{m''*}(\eta, \nu) & \text{for } r > R, \end{cases} \end{aligned}$$

where  $\gamma$  is the angle between vectors  $\vec{R}$  and  $\vec{r}$  (see Fig. 8).

As a result, we have

$$\begin{aligned} V_{e^- - M, x}^{\text{el}} &= ed_x \frac{\partial}{\partial R_x} \frac{1}{(R^2 + r^2 - 2rR \cos \gamma)^{1/2}} = \tag{A1} \\ &= 4\pi ed_x \sin \eta \cos \nu \begin{cases} \sum_{l''=0}^{\infty} -\frac{l''+1}{2l''+1} \frac{r^{l''}}{R^{l''+2}} \sum_{m''=-l''}^{l''} Y_{l''}^{m''}(\theta, \phi) Y_{l''}^{m''*}(\eta, \nu) & \text{for } r < R \\ \sum_{l''=0}^{\infty} \frac{l''}{2l''+1} \frac{R^{l''-1}}{r^{l''+1}} \sum_{m''=-l''}^{l''} Y_{l''}^{m''}(\theta, \phi) Y_{l''}^{m''*}(\eta, \nu) & \text{for } r > R \end{cases} \\ &+ 4\pi ed_x \frac{\cos \eta \cos \nu}{R} \begin{cases} \sum_{l''=0}^{\infty} \frac{1}{2l''+1} \frac{r^{l''}}{R^{l''+1}} \sum_{m''=-l''}^{l''} Y_{l''}^{m''}(\theta, \phi) \frac{\partial Y_{l''}^{m''*}(\eta, \nu)}{\partial \eta} & \text{for } r < R \\ \sum_{l''=0}^{\infty} \frac{1}{2l''+1} \frac{R^{l''}}{r^{l''+1}} \sum_{m''=-l''}^{l''} Y_{l''}^{m''}(\theta, \phi) \frac{\partial Y_{l''}^{m''*}(\eta, \nu)}{\partial \eta} & \text{for } r > R \end{cases} \\ &+ 4\pi i ed_x \frac{\sin \nu}{R \sin \eta} \begin{cases} \sum_{l''=0}^{\infty} \frac{1}{2l''+1} \frac{r^{l''}}{R^{l''+1}} \sum_{m''=-l''}^{l''} m'' Y_{l''}^{m''}(\theta, \phi) Y_{l''}^{m''*}(\eta, \nu) & \text{for } r < R \\ \sum_{l''=0}^{\infty} \frac{1}{2l''+1} \frac{R^{l''}}{r^{l''+1}} \sum_{m''=-l''}^{l''} m'' Y_{l''}^{m''}(\theta, \phi) Y_{l''}^{m''*}(\eta, \nu) & \text{for } r > R, \end{cases} \end{aligned}$$

$$\begin{aligned}
V_{e^{-M}, y}^{\text{el}} &= ed_y \frac{\partial}{\partial R_y} \frac{1}{(R^2 + r^2 - 2rR \cos \gamma)^{1/2}} = \tag{A2} \\
&= 4\pi ed_y \sin \eta \sin \nu \left\{ \begin{array}{l} \sum_{l''=0}^{\infty} -\frac{l''+1}{2l''+1} \frac{r^{l''}}{R^{l''+2}} \sum_{m''=-l''}^{l''} Y_{l''}^{m''}(\theta, \phi) Y_{l''}^{m''*}(\eta, \nu) \text{ for } r < R \\ \sum_{l''=0}^{\infty} \frac{l''}{2l''+1} \frac{R^{l''-1}}{r^{l''+1}} \sum_{m''=-l''}^{l''} Y_{l''}^{m''}(\theta, \phi) Y_{l''}^{m''*}(\eta, \nu) \text{ for } r > R \end{array} \right. \\
&\quad + 4\pi ed_y \frac{\cos \eta \sin \nu}{R} \left\{ \begin{array}{l} \sum_{l''=0}^{\infty} \frac{1}{2l''+1} \frac{r^{l''}}{R^{l''+1}} \sum_{m''=-l''}^{l''} Y_{l''}^{m''}(\theta, \phi) \frac{\partial Y_{l''}^{m''*}(\eta, \nu)}{\partial \eta} \text{ for } r < R \\ \sum_{l''=0}^{\infty} \frac{1}{2l''+1} \frac{R^{l''}}{r^{l''+1}} \sum_{m''=-l''}^{l''} Y_{l''}^{m''}(\theta, \phi) \frac{\partial Y_{l''}^{m''*}(\eta, \nu)}{\partial \eta} \text{ for } r > R \end{array} \right. \\
&\quad - 4\pi i ed_y \frac{\cos \nu}{R \sin \eta} \left\{ \begin{array}{l} \sum_{l''=0}^{\infty} \frac{1}{2l''+1} \frac{r^{l''}}{R^{l''+1}} \sum_{m''=-l''}^{l''} m'' Y_{l''}^{m''}(\theta, \phi) Y_{l''}^{m''*}(\eta, \nu) \text{ for } r < R \\ \sum_{l''=0}^{\infty} \frac{1}{2l''+1} \frac{R^{l''}}{r^{l''+1}} \sum_{m''=-l''}^{l''} m'' Y_{l''}^{m''}(\theta, \phi) Y_{l''}^{m''*}(\eta, \nu) \text{ for } r > R, \end{array} \right.
\end{aligned}$$

$$\begin{aligned}
V_{e^{-M}, z}^{\text{el}} &= ed_z \frac{\partial}{\partial R_z} \frac{1}{(R^2 + r^2 - 2rR \cos \gamma)^{1/2}} = \tag{A3} \\
&= 4\pi ed_z \cos \eta \left\{ \begin{array}{l} \sum_{l''=0}^{\infty} -\frac{l''+1}{2l''+1} \frac{r^{l''}}{R^{l''+2}} \sum_{m''=-l''}^{l''} Y_{l''}^{m''}(\theta, \phi) Y_{l''}^{m''*}(\eta, \nu) \text{ for } r < R \\ \sum_{l''=0}^{\infty} \frac{l''}{2l''+1} \frac{R^{l''-1}}{r^{l''+1}} \sum_{m''=-l''}^{l''} Y_{l''}^{m''}(\theta, \phi) Y_{l''}^{m''*}(\eta, \nu) \text{ for } r > R \end{array} \right. \\
&\quad - 4\pi ed_z \frac{\sin \eta}{R} \left\{ \begin{array}{l} \sum_{l''=0}^{\infty} \frac{1}{2l''+1} \frac{r^{l''}}{R^{l''+1}} \sum_{m''=-l''}^{l''} Y_{l''}^{m''}(\theta, \phi) \frac{\partial Y_{l''}^{m''*}(\eta, \nu)}{\partial \eta} \text{ for } r < R \\ \sum_{l''=0}^{\infty} \frac{1}{2l''+1} \frac{R^{l''}}{r^{l''+1}} \sum_{m''=-l''}^{l''} Y_{l''}^{m''}(\theta, \phi) \frac{\partial Y_{l''}^{m''*}(\eta, \nu)}{\partial \eta} \text{ for } r > R, \end{array} \right.
\end{aligned}$$

where

$$\frac{\partial Y_{l''}^{m''*}(\eta, \nu)}{\partial \eta} = -\frac{1}{2} \left( \sqrt{(l'' + m'')(l'' - m'' + 1)} (Y_{l''}^{m''-1})^* e^{-i\nu} - \sqrt{(l'' - m'')(l'' + m'' + 1)} (Y_{l''}^{m''+1})^* e^{i\nu} \right).$$

## 2. Calculation of the interaction matrix elements Eq. (2) in the case $\vec{R} = R\vec{e}_z$

We can obtain the interaction matrix elements in the case  $\vec{R} = R\vec{e}_z$  by taking the limit  $\eta \rightarrow 0$ ,  $\nu \rightarrow 0$  in Eqs.(A1)-(A3). In this limit  $Y_{l''}^{m''}(\eta, \nu) \rightarrow \sqrt{\frac{2l''+1}{4\pi}} \delta_{m'',0}$  and  $Y_{l''}^{m''}(\theta, \phi) \frac{\partial Y_{l''}^{m''*}(\eta, \nu)}{\partial \eta} \rightarrow -\frac{1}{2} \sqrt{\frac{(2l''+1)l''(l''+1)}{4\pi}} (Y_{l''}^1(\theta, \phi) - Y_{l''}^{-1}(\theta, \phi))$ .

As a result,  $V_{e^{-M}}^{\text{core}} = \frac{ed_z}{R^2}$ ,

$$V_{e^{-M}, x}^{\text{el}} = -\frac{ed_x}{2R} \left\{ \begin{array}{l} \sum_{l''=0}^{\infty} \sqrt{\frac{4\pi l''(l''+1)}{2l''+1}} \frac{r^{l''}}{R^{l''+1}} (Y_{l''}^1(\theta, \phi) - Y_{l''}^{-1}(\theta, \phi)) \text{ for } r < R \\ \sum_{l''=0}^{\infty} \sqrt{\frac{4\pi l''(l''+1)}{2l''+1}} \frac{R^{l''}}{r^{l''+1}} (Y_{l''}^1(\theta, \phi) - Y_{l''}^{-1}(\theta, \phi)) \text{ for } r > R. \end{array} \right.$$

Next, when  $\eta \rightarrow 0, \nu \rightarrow 0$

$$V_{e^{-M}, y}^{\text{el}} \rightarrow -\frac{4\pi i ed_y}{R \sin \eta} \left\{ \begin{array}{l} \sum_{l''=0}^{\infty} \frac{1}{2l''+1} \frac{r^{l''}}{R^{l''+1}} (Y_{l''}^1(\theta, \phi) Y_{l''}^{1*}(\eta, \nu) - Y_{l''}^{-1}(\theta, \phi) Y_{l''}^{-1*}(\eta, \nu)) \text{ for } r < R \\ \sum_{l''=0}^{\infty} \frac{1}{2l''+1} \frac{R^{l''}}{r^{l''+1}} (Y_{l''}^1(\theta, \phi) Y_{l''}^{1*}(\eta, \nu) - Y_{l''}^{-1}(\theta, \phi) Y_{l''}^{-1*}(\eta, \nu)) \text{ for } r > R \end{array} \right.$$

and we can use the small  $\eta$  approximation  $Y_{l''}^1(\eta, 0) \rightarrow -\frac{\sin \eta}{2} \sqrt{\frac{(2l''+1)l''(l''+1)}{4\pi}}$ , giving

$$V_{e^{-M}, y}^{\text{el}} = \frac{i ed_y}{2R} \left\{ \begin{array}{l} \sum_{l''=0}^{\infty} \sqrt{\frac{4\pi l''(l''+1)}{2l''+1}} \frac{r^{l''}}{R^{l''+1}} (Y_{l''}^1(\theta, \phi) + Y_{l''}^{-1}(\theta, \phi)) \text{ for } r < R \\ \sum_{l''=0}^{\infty} \sqrt{\frac{4\pi l''(l''+1)}{2l''+1}} \frac{R^{l''}}{r^{l''+1}} (Y_{l''}^1(\theta, \phi) + Y_{l''}^{-1}(\theta, \phi)) \text{ for } r > R, \end{array} \right.$$

resulting in

$$V_{e^{-}M, x}^{\text{el}} + V_{e^{-}M, y}^{\text{el}} = -\frac{e(d_x - id_y)}{2R} \begin{cases} \sum_{l''=0}^{\infty} \sqrt{\frac{4\pi l''(l''+1)}{2l''+1}} \frac{r^{l''}}{R^{l''+1}} Y_{l''}^1(\theta, \phi) & \text{for } r < R \\ \sum_{l''=0}^{\infty} \sqrt{\frac{4\pi l''(l''+1)}{2l''+1}} \frac{R^{l''}}{r^{l''+1}} Y_{l''}^1(\theta, \phi) & \text{for } r > R \end{cases} \\ + \frac{e(d_x + id_y)}{2R} \begin{cases} \sum_{l''=0}^{\infty} \sqrt{\frac{4\pi l''(l''+1)}{2l''+1}} \frac{r^{l''}}{R^{l''+1}} Y_{l''}^{-1}(\theta, \phi) & \text{for } r < R \\ \sum_{l''=0}^{\infty} \sqrt{\frac{4\pi l''(l''+1)}{2l''+1}} \frac{R^{l''}}{r^{l''+1}} Y_{l''}^{-1}(\theta, \phi) & \text{for } r > R, \end{cases}$$

$$V_{e^{-}M, z}^{\text{el}} = ed_z \begin{cases} \sum_{l''=0}^{\infty} -\sqrt{\frac{4\pi}{2l''+1}} (l''+1) \frac{r^{l''}}{R^{l''+2}} Y_{l''}^0(\theta, \phi) & \text{for } r < R \\ \sum_{l''=0}^{\infty} \sqrt{\frac{4\pi}{2l''+1}} l'' \frac{R^{l''-1}}{r^{l''+1}} Y_{l''}^0(\theta, \phi) & \text{for } r > R. \end{cases}$$

Next we will analyze separately the three terms of  $V_{e^{-}M}$ :

1) The matrix element of the interaction between the molecular dipole and the Rydberg core has the form:

$$(V_{e^{-}M}^{\text{core}})_{nlmJm_J, n'l'm'_Jm'_J} = \langle J, m_J | \langle n l m | \frac{ed_z}{R^2} | n' l' m' \rangle | J' m'_J \rangle = \frac{ed_z^{J, m_J; J', m'_J}}{R^2} \delta_{n, n'} \delta_{l, l'} \delta_{m, m'} \delta_{J \pm 1, J'} \delta_{m_J, m'_J}, \quad (\text{A4})$$

2) The matrix elements of the  $V_{e^{-}M, z}^{\text{el}}$  and  $V_{e^{-}M, x}^{\text{el}} + V_{e^{-}M, y}^{\text{el}}$  terms have the form:

$$\langle J, m_J | \langle n l m | V_{e^{-}M, z}^{\text{el}} | n' l' m' \rangle | J', m'_J \rangle = \quad (\text{A5}) \\ = \delta_{m, m'} \left( - \sum_{l''=0}^{\infty} (l''+1) \sqrt{\frac{4\pi}{2l''+1}} \frac{1}{R^{l''+2}} \int_0^R r^{l''+2} R_{nl}(r) R_{n'l'}(r) dr \int_0^{2\pi} d\phi \int_0^\pi Y_l^{m*} Y_{l''}^0 Y_{l'}^{m'} \sin \theta d\theta + \right. \\ \left. + \sum_{l''=0}^{\infty} l'' \sqrt{\frac{4\pi}{2l''+1}} R^{l''-1} \int_R^\infty \frac{1}{r^{l''-1}} R_{nl}(r) R_{n'l'}(r) dr \int_0^{2\pi} d\phi \int_0^\pi Y_l^{m*} Y_{l''}^0 Y_{l'}^{m'} \sin \theta d\theta \right) \langle J, m_J | ed_z | J', m'_J \rangle = \\ = \delta_{m, m'} \delta_{J', J \pm 1} \delta_{m_J, m'_J} \left( - \sum_{l''=0}^{\infty} (l''+1) \sqrt{\frac{4\pi}{2l''+1}} \frac{1}{R^{l''+2}} \int_0^R r^{l''+2} R_{nl}(r) R_{n'l'}(r) dr \int_0^\pi Y_l^{m*} Y_{l''}^0 Y_{l'}^m \sin \theta d\theta + \right. \\ \left. + \sum_{l''=0}^{\infty} l'' \sqrt{\frac{4\pi}{2l''+1}} R^{l''-1} \int_R^\infty \frac{1}{r^{l''-1}} R_{nl}(r) R_{n'l'}(r) dr \int_0^\pi Y_l^{m*} Y_{l''}^0 Y_{l'}^m \sin \theta d\theta \right) ed_z^{J, m_J; J', m'_J}$$

and,

$$\begin{aligned}
& \langle J, m_J | \langle n l m | V_{e^{-M}, x}^{\text{el}} + V_{e^{-M}, y}^{\text{el}} | n' l' m' \rangle | J', m'_J \rangle = \\
& = - \left( \sum_{l''=0}^{\infty} \frac{1}{R^{l''+1}} \sqrt{\frac{4\pi l''(l''+1)}{2l''+1}} \int_0^R r^{l''+2} R_{nl}(r) R_{n'l'} dr \int_0^{2\pi} d\phi \int_0^\pi Y_l^{m*} Y_{l''}^1 Y_{l'}^{m'} \sin \theta d\theta + \right. \\
& + \sum_{l''=0}^{\infty} R^{l''} \sqrt{\frac{4\pi l''(l''+1)}{2l''+1}} \int_R^\infty \frac{R_{nl} R_{n'l'}}{r^{l''-1}} dr \int_0^{2\pi} d\phi \int_0^\pi Y_l^{m*} Y_{l''}^1 Y_{l'}^{m'} \sin \theta d\theta \left. \right) \frac{e \langle J, m_J | d_x - i d_y | J', m'_J \rangle}{2R} \\
& + \left( \sum_{l''=0}^{\infty} \frac{1}{R^{l''+1}} \sqrt{\frac{4\pi l''(l''+1)}{2l''+1}} \int_0^R r^{l''+2} R_{nl}(r) R_{n'l'} dr \int_0^{2\pi} d\phi \int_0^\pi Y_l^{m*} Y_{l''}^{-1} Y_{l'}^{m'} \sin \theta d\theta + \right. \\
& + \sum_{l''=0}^{\infty} R^{l''} \sqrt{\frac{4\pi l''(l''+1)}{2l''+1}} \int_R^\infty \frac{R_{nl} R_{n'l'}}{r^{l''-1}} dr \int_0^{2\pi} d\phi \int_0^\pi Y_l^{m*} Y_{l''}^{-1} Y_{l'}^{m'} \sin \theta d\theta \left. \right) \frac{e \langle J, m_J | d_x + i d_y | J', m'_J \rangle}{2R} = \\
& = - \frac{e d_+^{J, m_J; J', m'_J}}{\sqrt{2}R} \delta_{m, m'+1} \left( \sum_{l''=0}^{\infty} \frac{1}{R^{l''+1}} \sqrt{\frac{4\pi l''(l''+1)}{2l''+1}} \int_0^R r^{l''+2} R_{nl}(r) R_{n'l'} dr \int Y_l^{m*} Y_{l''}^1 Y_{l'}^{m'} \sin \theta' d\theta' d\phi' + \right. \\
& + \sum_{l''=0}^{\infty} R^{l''} \sqrt{\frac{4\pi l''(l''+1)}{2l''+1}} \int_R^\infty \frac{R_{nl} R_{n'l'}}{r^{l''-1}} dr \int Y_l^{m*} Y_{l''}^1 Y_{l'}^{m'} \sin \theta' d\theta' d\phi' \left. \right) \\
& - \frac{e d_-^{J, m_J; J', m'_J}}{\sqrt{2}R} \delta_{m, m'-1} \left( \sum_{l''=0}^{\infty} \frac{1}{R^{l''+1}} \sqrt{\frac{4\pi l''(l''+1)}{2l''+1}} \int_0^R r^{l''+2} R_{nl}(r) R_{n'l'} dr \int Y_l^{m*} Y_{l''}^{-1} Y_{l'}^{m'} \sin \theta' d\theta' d\phi' + \right. \\
& + \sum_{l''=0}^{\infty} R^{l''} \sqrt{\frac{4\pi l''(l''+1)}{2l''+1}} \int_R^\infty \frac{R_{nl} R_{n'l'}}{r^{l''-1}} dr \int Y_l^{m*} Y_{l''}^{-1} Y_{l'}^{m'} \sin \theta' d\theta' d\phi' \left. \right),
\end{aligned}$$

where the dipole moment matrix elements are  $d_z^{J m_J, J' m'_J} = \langle J, m_J | d_z | J', m'_J \rangle$ ,  $d_\pm^{J m_J, J' m'_J} = \pm \langle J, m_J | d_x \mp i d_y | J', m'_J \rangle / \sqrt{2}$ , where for  $J = 0$ ,  $J = 1$  and  $J = 2$  rotational states the corresponding matrix elements are  $d_z^{0,0;1,0} = d/\sqrt{3}$ ,  $d_z^{1,0;2,0} = 2d/\sqrt{15}$ ,  $d_z^{1,\pm 1;2,\pm 1} = d/\sqrt{5}$ ,  $d_\pm^{0,0;1,\pm 1} = -d/\sqrt{3}$ ,  $d_\pm^{1,0;2,\pm 1} = -d/\sqrt{5}$ ,  $d_\pm^{1,\pm 1;2,\pm 2} = -d\sqrt{2}/\sqrt{5}$ ,  $d_\pm^{1,\pm 1;2,0} = -d/\sqrt{15}$ , where  $d$  is the permanent dipole moment of a molecule. The integrals involving three spherical harmonics are calculated using the expression:

$$\begin{aligned}
& \int_0^{2\pi} \int_0^\pi Y_{l_1}^{m_1}(\theta, \phi) Y_{l_2}^{m_2}(\theta, \phi) Y_{l_3}^{m_3}(\theta, \phi) \sin \theta d\theta d\phi = \\
& = \sqrt{\frac{(2l_1+1)(2l_2+1)(2l_3+1)}{4\pi}} \begin{pmatrix} l_1 & l_2 & l_3 \\ 0 & 0 & 0 \end{pmatrix} \begin{pmatrix} l_1 & l_2 & l_3 \\ m_1 & m_2 & m_3 \end{pmatrix}.
\end{aligned}$$

where  $\begin{pmatrix} l_1 & l_2 & l_3 \\ m_1 & m_2 & m_3 \end{pmatrix}$  is the 3j-symbol.

The matrix elements of the full Hamiltonian including all terms are then given by

$$\begin{aligned}
& \langle J, m_J | \langle n l m | H | n' l' m' \rangle | J', m'_J \rangle = \\
& = - \frac{1}{2(n-\mu)^2} \delta_{n, n'} \delta_{l, l'} \delta_{m, m'} \delta_{J, J'} \delta_{m_J, m'_J} + B J(J+1) \delta_{n, n'} \delta_{l, l'} \delta_{m, m'} \delta_{J, J'} \delta_{m_J, m'_J} \\
& + \langle J, m_J | \langle n l m | V_{e^{-M}}^{\text{core}} | n' l' m' \rangle | J', m'_J \rangle + \sum_{\alpha=x, y, z} \langle J, m_J | \langle n l m | V_{e^{-M}, \alpha}^{\text{el}} | n' l' m' \rangle | J', m'_J \rangle.
\end{aligned}$$

The total Hamiltonian is then diagonalized to find new eigenstates accounting for the interaction, and corresponding eigenenergies.

### 3. Calculation of the matrix elements for the case $\vec{R} = R_x \vec{e}_x + R_z \vec{e}_z$ using $|60s\rangle$ atomic and $|J = 0, m_J = 0\rangle$ , $|J = 1, m_J = 0\rangle$ molecular basis states

The case  $R_y = 0$  corresponds to the limit  $\nu = 0$  in Eqs.(A1)-(A3). These expressions are further simplified by using only the  $|ns\rangle$  atomic basis state. In the matrix elements  $\langle ns | V_{e^{-M}, \alpha} | ns \rangle \sim$

$\int_0^{2\pi} d\phi \int_0^\pi Y_0^{0*}(\theta, \phi) Y_l^{m''}(\theta, \phi) Y_0^0(\theta, \phi) \sin \theta d\theta$  only  $l'' = 0, m'' = 0$  terms are non-zero. As a result,  $\frac{\partial Y_{l''=0}^{m''=0*}(\eta, 0)}{\partial \eta} = 0$  and the interaction terms have the form:

$$V_{e^-M, z}^{\text{el}} = 4\pi e d_z \cos \eta \begin{cases} -\frac{1}{R^2} Y_0^0(\theta, \phi) & \text{for } r < R \\ 0 & \text{for } r > R \end{cases}$$

$$V_{e^-M, x}^{\text{el}} = 4\pi e d_x \sin \eta \begin{cases} -\frac{1}{R^2} Y_0^0(\theta, \phi) & \text{for } r < R \\ 0 & \text{for } r > R \end{cases}$$

and  $V_{e^-M, y}^{\text{el}} = 0$ . Finally, using only  $|J = 0, m_J = 0\rangle$  and  $|J = 1, m_J = 0\rangle$  molecular basis states allows us to neglect the  $V_{e^-M, x}^{\text{el}} \sim \langle J = 0, m_J | d_x | J = 1, m_J = 0 \rangle = 0$  term, as well as the  $ed_x R_x / R^3$  term in  $V_{e^-M}^{\text{core}}$ . We are therefore left with the only non-zero matrix element

$$\langle J = 0, m_J = 0 | \langle ns | V_{e^-M} | ns \rangle | J = 1, m_J = 0 \rangle = \frac{ed_z^{0,0;1,0} \cos \eta}{R^2} - d_z^{0,0;1,0} \cos \eta \frac{1}{R^2} \int_0^R r^2 R_{ns}^2 dr.$$

## Appendix B

In this section we show that interaction matrix elements between states  $|ns\rangle |\downarrow\rangle = |ns\rangle |J = 0, m_J = 0\rangle$ ,  $|ns\rangle |\uparrow\rangle = |ns\rangle |J = 1, m_J = 0, \pm 1\rangle$  and their closest in energy neighbours are much smaller than the energy difference between the corresponding states. The corresponding level schemes are shown in Fig. 9a and b for KRb and c and d for RbYb, respectively. We consider the case  $\vec{R} = R\vec{e}_z$  analyzed in part (2) of Appx. A.

The matrix elements  $\langle V_{e^-M} \rangle = \langle J = 0, m_J = 0 | \langle ns | V_{e^-M} | n'l'm' \rangle | J' = 1, m'_J \rangle$ , where  $m'_J + m' = 0$  by selection rules, are shown in Fig. 10a and b for KRb and RbYb, respectively. The matrix elements  $\langle J = 1, m_J | \langle ns | V_{e^-M} | n'l'm' \rangle | J' = 2, m'_J \rangle$  (with  $m_J = m' + m'_J$  and  $m'_J = m_J, m_J \pm 1$ ) describing transitions between  $J = 1$  and  $J = 2$  rotational states can be expressed via the corresponding  $J = 0 \leftrightarrow J = 1$  matrix elements as  $\langle J = 1, m_J | \langle ns | V_{e^-M, \alpha} | n'l'm' \rangle | J' = 2, m'_J \rangle = \left( d_\alpha^{1, m_J; 2, m'_J} / d_\alpha^{0, 0; 1, m'_J - m_J} \right) \langle J = 0, m_J = 0 | \langle ns | V_{e^-M, \alpha} | n'l'm' \rangle | J' = 1, m'_J - m_J \rangle$ , where  $\alpha = z, \pm$  and  $\left| d_\alpha^{1, m_J; 2, m'_J} / d_\alpha^{0, 0; 1, m'_J - m_J} \right| \sim 1$  as can be seen from the end of part (2) of Appx. A. From Figs. 9 and 10 one can see that  $\left| V_{e^-M}^{ns, J, m_J; n'l'm', J', m'_J} / (E_{ns, J, m_J} - E_{n'l'm', J', m'_J}) \right| < 0.03$  for KRb for both  $J = 0$  and  $J = 1$  rotational states and all closest in energy states  $|n'l'm'\rangle$  (this ratio is  $< 0.08$  for RbYb). In particular, this validates the discussion in Section III about the small effect of possible spin-rotation splitting of  $J = 1$  states of RbYb on the energy shifts. For both KRb and RbYb the most important contribution to the energy shift of the  $|ns\rangle |J = 0, m_J = 0\rangle$  state comes from the interaction with the  $|ns\rangle |J = 1, m_J = 0\rangle$  state; for the  $|ns\rangle |J = 1, m_J = 0\rangle$  the largest contribution is from interaction with  $|ns\rangle |J = 0, m_J = 0\rangle$  and  $|ns\rangle |J = 2, m_J = 0\rangle$  states; for the  $|ns\rangle |J = 1, m_J = \pm 1\rangle$  the main contributions of the same amount and opposite sign come from interaction with  $|ns\rangle |J = 2, m_J = \pm 1\rangle$  and  $|(n-2)d, m\rangle |J = 2, m_J = 0, \pm 1, \pm 2\rangle$  states.

## Appendix C

In this section we discuss the convergence of the calculations of the energy shifts shown in Fig. 2 with respect to the atomic and molecular basis states. We checked if all the states  $np$ ,  $(n-1)p$ ,  $(n-1)d$ ,  $(n-2)d$  and  $(n-3)f$  are contributing significantly to the energy shifts. Figs. 11a and b show the shifts taking into account the full set of 60s, 60p, 59p, 59d, 58d and 57f states (thick lines) and and three closest in energy 60p, 59p and 58d states (thin lines) for KRb and RbYb, respectively. One can see that for both KRb and RbYb the smaller basis set gives a good agreement with the full one except for the  $|J = 1, m_J = 0\rangle$  state. We also compared the shifts calculated using the full set and the smallest possible atomic set including only the 60s state. It will give a good approximation to the full set if  $|\langle J = 0, m_J = 0 | \langle ns | V_{e^-M} | ns \rangle | J' = 1, m'_J \rangle|^2 / 2B \gg |\langle J, m_J | \langle ns | V_{e^-M} | n'(l' > 0)m' \rangle | J', m'_J \rangle|^2 / |E_{ns, J, m_J} - E_{n'(l' > 0)m', J', m'_J}|$ . The results are shown in Fig. 11c and d for KRb and RbYb, respectively. Again, for RbYb the smallest set has a good agreement with the full one except for the  $|J = 1, m_J = 0\rangle$  state. For KRb the smallest and the full sets agree approximately, giving shifts of the same order of magnitude and sign except for the  $|J = 1, m_J = \pm 1\rangle$  states.

The effect of the 57f state can be seen in Fig. 2a and b for KRb and RbYb, respectively. The thick lines show the shifts calculated using the full set, and the thin lines correspond to shifts calculated without the 57f state. One can see that the effect of the f state is reasonably small. For RbYb the curves with and without 57f completely overlap.

The above calculations were done taking into account  $J = 0, 1, 2$  rotational states. We also checked if higher rotational states such as  $|J = 3, m_J = 0, \pm 1, \pm 2, \pm 3\rangle$  influence the shifts. Fig. 11e and f compare the shifts for KRb and RbYb, respectively, using the smaller basis set of  $60s, 60p, 59p, 58d$  to simplify the calculations and  $J = 0, 1, 2$  (thick curves) and  $J = 0, 1, 2, 3$  (thin curves) rotational states. One can see that the curves completely overlap, which means that the shifts of the  $J = 0$  and  $J = 1$  rotational states are hardly affected by the  $J = 3$  states.

## Appendix D

In this section we estimate the effect of a finite spread of atomic and molecular positions in their respective traps on the energy shifts obtained in Section III and IV. For that we assume both the Rydberg atom and the molecule to be in a ground state of their harmonic traps and approximate the corresponding wavefunctions as  $\Psi_{\text{at(mol)}}(\vec{\mathcal{R}}_{\text{at(mol)}}) = \exp\left(-(\mathcal{R}_{\text{at(mol)}})^2/2a_{\text{ho at(mol)}}^2\right)/(\pi a_{\text{ho at(mol)}}^2)^{1/4}$ , where  $\vec{\mathcal{R}}_{\text{at(mol)}}$  is the position of the atom(molecule) with respect to its trap center,  $a_{\text{ho at(mol)}}$  is the corresponding wavefunction width. In Appx. B it was shown that the main contributions to the shifts of the  $|ns\rangle|J = 0, m_J = 0\rangle$  and  $|ns\rangle|J = 1, m_J = 0\rangle$  come from the interaction with other  $|ns\rangle|J', m_J'\rangle$  states. For the  $|ns\rangle|J = 1, m_J = \pm 1\rangle$  both the  $|ns\rangle|J = 2, m_J = \pm 1\rangle$  and  $|(n-2)d, m\rangle|J = 2, m_J = 0, \pm 1, \pm 2\rangle$  states contribute significantly. The interaction matrix elements for  $ns$  states can be written as follows

$$V_{e^- - M}^{nsJm_J; nsJ'm_J'} = \frac{c_{nsJm_J; nsJ'm_J'}}{(\rho + \mathcal{R}_z \text{ mol} - \mathcal{R}_z \text{ at})^2 + (\mathcal{R}_x \text{ mol} - \mathcal{R}_x \text{ at})^2 + (\mathcal{R}_y \text{ mol} - \mathcal{R}_y \text{ at})^2}, \quad (\text{D1})$$

where  $c_{nsJm_J; nsJ'm_J'}$  is a constant coefficient. The matrix element between  $|ns\rangle|J = 1, m_J = \pm 1\rangle$  and  $|(n-2)d, m\rangle|J', m_J'\rangle$  states has the following form:

$$V_{e^- - M}^{nsJm_J; (n-2)mdJ'm_J'} = \frac{c_{nsJm_J; (n-2)mdJ'm_J'}}{((\rho + \mathcal{R}_z \text{ mol} - \mathcal{R}_z \text{ at})^2 + (\mathcal{R}_x \text{ mol} - \mathcal{R}_x \text{ at})^2 + (\mathcal{R}_y \text{ mol} - \mathcal{R}_y \text{ at})^2)^2}. \quad (\text{D2})$$

The matrix elements Eqs. (D1) and (D2) should be multiplied by  $|\Psi_{\text{at(mol)}}|^2$  and averaged over atomic and molecular positions:

$$\langle V_{e^- - M}^{nsJm_J; nsJ'm_J'} \rangle = \frac{c_{nsJm_J; nsJ'm_J'}}{\pi^3 a_{\text{ho at}}^3 a_{\text{ho mol}}^3} \int \frac{\exp(-(\mathcal{R}_{\text{at}})^2/a_{\text{ho at}}^2) \exp(-(\mathcal{R}_{\text{mol}})^2/a_{\text{ho mol}}^2)}{(\rho + \mathcal{R}_z \text{ mol} - \mathcal{R}_z \text{ at})^2 + (\mathcal{R}_x \text{ mol} - \mathcal{R}_x \text{ at})^2 + (\mathcal{R}_y \text{ mol} - \mathcal{R}_y \text{ at})^2} d^3\vec{\mathcal{R}}_{\text{at}} d^3\vec{\mathcal{R}}_{\text{mol}} \quad (\text{D3})$$

and the same averaging should be done for  $V_{e^- - M}^{nsJm_J; (n-2)mdJ'm_J'}$ .

Let us introduce the integration variables  $\vec{\mathcal{R}}^p = (\vec{\mathcal{R}}_{\text{mol}} + \vec{\mathcal{R}}_{\text{at}})/2$ ,  $\vec{\mathcal{R}}^m = \vec{\mathcal{R}}_{\text{mol}} - \vec{\mathcal{R}}_{\text{at}}$  with the inverse relations  $\vec{\mathcal{R}}_{\text{mol}} = \vec{\mathcal{R}}^p + \vec{\mathcal{R}}^m/2$ ,  $\vec{\mathcal{R}}_{\text{at}} = \vec{\mathcal{R}}^p - \vec{\mathcal{R}}^m/2$ , giving  $d^3\vec{\mathcal{R}}_{\text{mol}} d^3\vec{\mathcal{R}}_{\text{at}} = d^3\vec{\mathcal{R}}^p d^3\vec{\mathcal{R}}^m$ . Let us also assume for simplicity that  $a_{\text{ho at}} = a_{\text{ho mol}} = a$ . In this case Eq. (D3) becomes

$$\langle V_{e^- - M}^{nsJm_J; nsJ'm_J'} \rangle = \frac{c_{nsJm_J; nsJ'm_J'}}{\pi^3 a^6} \int \frac{\exp(-2(\mathcal{R}^p)^2/a^2 - (\mathcal{R}^m)^2/2a^2)}{(\rho + \mathcal{R}_z^m)^2 + (\mathcal{R}_x^m)^2 + (\mathcal{R}_y^m)^2} d^3\vec{\mathcal{R}}^p d^3\vec{\mathcal{R}}^m.$$

The integration over  $\vec{\mathcal{R}}^p$  is straightforward and gives unity. In order to carry the integration over  $\vec{\mathcal{R}}^m$  we assume that  $\rho \gg a$  and expand the denominator in  $\mathcal{R}_x^m/\rho$ ,  $\mathcal{R}_y^m/\rho$ ,  $\mathcal{R}_z^m/\rho$  up to second order:

$$\frac{1}{(\rho + \mathcal{R}_z^m)^2 + (\mathcal{R}_x^m)^2 + (\mathcal{R}_y^m)^2} \approx \frac{1}{\rho^2} \left( 1 - \frac{2\mathcal{R}_z^m}{\rho} + 3 \left( \frac{\mathcal{R}_z^m}{\rho} \right)^2 - \left( \frac{\mathcal{R}_x^m}{\rho} \right)^2 - \left( \frac{\mathcal{R}_y^m}{\rho} \right)^2 \right).$$

The integration over  $\vec{\mathcal{R}}^m$  then gives the following result:

$$\langle V_{e^- - M}^{nsJm_J; nsJ'm_J'} \rangle \approx \frac{c_{nsJm_J; nsJ'm_J'}}{\rho^2} \left( 1 + \frac{a^2}{\rho^2} \right).$$

The same procedure results in

$$V_{e^- - M}^{nsJm_J; (n-2)mdJ'm_J'} \approx \frac{c_{nsJm_J; (n-2)mdJ'm_J'}}{\rho^4} \left( 1 + 6 \frac{a^2}{\rho^2} \right).$$

Finally, the energy shifts of the states  $|ns\rangle |J = 0, m_J = 0\rangle$ ,  $|ns\rangle |J = 1, m_J = 0\rangle$ , and  $|ns\rangle |J = 1, m_J = \pm 1\rangle$  will have the form:

$$\begin{aligned} \Delta E_{ns,0,0} &\approx \frac{|V_{e^-M}^{ns,0,0;ns,1,0}|^2}{E_{ns,0,0} - E_{ns,1,0}} \approx -\frac{|c_{ns,0,0;ns,1,0}|^2}{\rho^4 E_{\text{rot}}} \left(1 + 2\frac{a^2}{\rho^2}\right), \\ \Delta E_{ns,1,0} &\approx \frac{|V_{e^-M}^{ns,1,0;ns,0,0}|^2}{E_{ns,1,0} - E_{ns,0,0}} + \frac{|V_{e^-M}^{ns,1,0;ns,2,0}|^2}{E_{ns,1,0} - E_{ns,2,0}} \approx \frac{|c_{ns,1,0;ns,0,0}|^2}{\rho^4 E_{\text{rot}}} \left(1 + 2\frac{a^2}{\rho^2}\right) - \frac{|c_{ns,1,0;ns,2,0}|^2}{\rho^4 2E_{\text{rot}}} \left(1 + 2\frac{a^2}{\rho^2}\right), \\ \Delta E_{ns,1,\pm 1} &\approx \frac{|V_{e^-M}^{ns,1,\pm 1;ns,2,\pm 1}|^2}{E_{ns,1,\pm 1} - E_{ns,2,\pm 1}} + \sum_{m,m'_J=0,\pm 1,\pm 2} \frac{|V_{e^-M}^{ns,1,\pm 1;(n-2)d,m,2,m'_J}|^2}{E_{ns,1,\pm 1} - E_{(n-2)d,m,2,m'_J}} \\ &\approx -\frac{|c_{ns,1,\pm 1;ns,2,\pm 1}|^2}{2E_{\text{rot}}\rho^4} \left(1 + 2\frac{a^2}{\rho^2}\right) + \sum_{m,m'_J=0,\pm 1,\pm 2} \frac{|c_{ns,1,\pm 1;(n-2)d,m,2,m'_J}|^2}{\rho^8 (E_{ns,1,\pm 1} - E_{(n-2)d,m,2,m'_J})} \left(1 + 12\frac{a^2}{\rho^2}\right), \end{aligned}$$

For sufficiently deep traps oscillation frequencies reach  $\omega_{\text{ho}} \sim 100$  kHz, resulting in  $a = \sqrt{\hbar/m\omega_{\text{ho}}} \leq 30$  nm, where  $m$  is the mass of Rb, KRb or RbYb. For KRb at  $\rho \geq 300$  nm it gives  $2(a/\rho)^2 \leq 2 \cdot 10^{-2}$ , for RbYb at  $\rho > 400$  nm the corresponding number is  $2(a/\rho)^2 \leq 10^{-2}$ . It allows to estimate the corrections to the energy shifts shown in Fig. 2 due to the finite spread of atomic and molecular positions in their traps. For KRb maximal energy shifts of the  $|J = 0, m_J = 0\rangle$  and  $|J = 1, m_J = 0\rangle$  states are  $\sim 1$  MHz, giving the correction  $\leq 20$  kHz. For RbYb the maximal energy shifts  $\sim 4$  MHz result in the energy correction  $\leq 40$  kHz. The correction to the energy shift of the  $|J = 1, m_J = \pm 1\rangle$  state can be calculated using interaction matrix elements discussed in Appx. B, giving the maximal correction  $\leq 60$  kHz for KRb and  $\leq 7$  kHz for RbYb. The same corrections apply to the energies of collective rotational states Eq. (7), which become  $\Delta E_{(k\uparrow,(N-k)\downarrow)} \approx -\frac{N-2k}{N_a^2} \frac{|V_{e^-M}^{j=i}|^2}{E_{\text{rot}}} \left(1 + 2\frac{a^2}{\rho^2}\right)$ , where we took into account that only  $ns$  state is used to calculate  $V_{e^-M}^{j=i}$ . It means that to the energy of each collective state the term  $\Delta E(k\uparrow,(N-k)\downarrow)(2a^2/\rho^2)$  is added. For the case of  $N = 3, 5$  molecules considered in Section IV, the corrections for the collective states is  $\leq 4$  kHz for KRb and  $\leq 10$  kHz for RbYb.

This energy correction has to be taken into account when the system is excited to the Rydberg state selectively for a particular rotational state because it can tune the excitation field out of resonance. The excitation field can be made resonant by e.g. making its Rabi frequency to be larger than the corresponding energy correction. Another solution is to excite the system with a chirped pulse such that its frequency sweep covers the corrected energy.

- 
- [1] D. DeMille, Phys. Rev. Lett. **88**, 067901 (2002); A. Andre, D. DeMille, J. M. Doyle, M. D. Lukin, S. E. Maxwell, P. Rabl, R. J. Shoelkopf, P. Zoller, Nat. Phys. **2**, 636 (2006); S. Yelin, K. Kirby, R. Cote, Phys. Rev. Lett. **74**, 050301 (2006).
  - [2] A. V. Gorshkov, S. R. Manmana, G. Chen, J. Ye, E. Demler, M. D. Lukin, A. M. Rey, Phys. Rev. Lett. **107**, 115301 (2011).
  - [3] S. R. Manmana, E. M. Stoudenmire, K. R. A. Hazzard, A. M. Rey, A. V. Gorshkov, Phys. Rev. A **87**, 081106(R) (2013).
  - [4] K. R. A. Hazzard, M. van den Worm, M. Foss-Feig, S. R. Manmana, E. G. Dalla Torre, T. Pfau, M. Kastner, A. M. Rey, Phys. Rev. A **90**, 063622 (2014).
  - [5] B. Yan, S. A. Moses, B. Gadway, J. P. Covey, K. R. A. Hazzard, A. M. Rey, D. S. Jin, J. Ye, Nature **501**, 521 (2013).
  - [6] A. de Paz, A. Sharma, A. Chotia, E. Marechal, J. H. Huckans, P. Pedri, L. Santos, O. Gorceix, L. Vernac, B. Laburthe-Tolra, Phys. Rev. Lett. **111**, 185305 (2013).
  - [7] W. C. Stwalley, H. Wang, J. Mol. Spectr. **195**, 194 (1999).
  - [8] F. Wolf, Y. Wan, J. C. Heip, F. Gebert, C. Shi, and P. O. Schmidt, Nature **530**, 457 (2016).
  - [9] E. Kuznetsova, S. T. Rittenhouse, H. R. Sadeghpour, S. F. Yelin, Phys. Chem. Chem. Phys. **13**, 17115 (2011).
  - [10] S. T. Rittenhouse, H. R. Sadeghpour, Phys. Rev. Lett. **104**, 243002 (2010);
  - [11] S. T. Rittenhouse, M. Mayle, P. Schmelcher, H. R. Sadeghpour, J. Phys. B **44**, 184005 (2011).
  - [12] L. Childress, M. V. Gurudev Dutt, J. M. Taylor, A. S. Zibrov, F. Jelezko, J. Wrachtrup, P. R. Hemmer, M. D. Lukin, Science **314**, 281 (2006).
  - [13] J. R. Petta, J. M. Taylor, A. C. Johnson, A. Yacoby, M. D. Lukin, C. M. Marcus, M. P. Hanson, A. C. Gossard, Phys. Rev. Lett. **100**, 067601 (2008).
  - [14] B. Urbaszek, X. Marie, T. Amand, O. Krebs, P. Voisin, P. Maletinsky, A. Hoge, A. Imamoglu, Rev. Mod. Phys. **85**, 79 (2013).
  - [15] E. M. Kessler, S. Yelin, M. D. Lukin, J. I. Cirac, G. Giedke, Phys. Rev. Lett. **104**, 143601 (2010).
  - [16] M. S. Rudner, L. M. K. Vandersypen, V. Vuletic, L. S. Levitov, Phys. Rev. Lett. **107**, 206806 (2011).
  - [17] G. Goldstein, P. Cappellaro, J. R. Maze, J. S. Hodges,

- L. Jiang, A. S. Sorensen, M. D. Lukin, Phys. Rev. Lett. **106**, 140502 (2011).
- [18] M. Schlagmiller, T. C. Liebisch, H. Nguyen, G. Lochead, F. Engel, F. Bttcher, K. M. Westphal, K. S. Kleinbach, R. Lw, S. Hofferberth, T. Pfau, Phys. Rev. Lett. **116**, 053001 (2016); R. Schmidt, H. R. Sadeghpour, E. Demler, Phys. Rev. Lett. **116**, 105302 (2016).
- [19] A. Gaj, A.T. Krupp, J.B. Balewski, R. Low, S. Hofferberth, T. Pfau, Nat. Comm. **5**, 4546 (2014).
- [20] H. Weimer, M. Mller, I. Lesanovsky, P. Zoller, H. P. Buchler, Nat. Phys. **6**, 382 (2010).
- [21] P. O. Schmidt, T. Rosenband, C. Langer, W. M. Itano, J. C. Bergquist, D. J. Wineland, Science **309**, 749 (2005); T. R. Tan, J. P. Gaebler, Y. Lin, Y. Wan, R. Bowler, D. Leibfried, D. J. Wineland, Nature **528**, 380 (2015); J. Mur-Petit, J. J. Garcia-Ripoll, J. Perez-Rios, J. Campos-Martinez, M. I. Hernandez, S. Willitsch, Phys. Rev. A **85**, 022308 (2012).
- [22] J. Mur-Petit, J. J. Garcia-Ripoll, Phys. Rev. A **91**, 012504 (2015); J. Mur-Petit, J. J. Garcia-Ripoll, Appl. Phys. B **114**, 283 (2014).
- [23] P. M. Preiss, R. Ma, M. E. Tai, J. Simon, M. Greiner, Phys. Rev. A **91**, 041602 (2015).
- [24] D. A. Anderson, S. A. Miller, G. Raithel, Phys. Rev. Lett. **112**, 163201 (2014).
- [25] W. Li, T. Pohl, J. M. Rost, S. T. Rittenhouse, H. R. Sadeghpour, J. Nipper, B. Butscher, J. B. Balewski, V. Bendkowsky, R. Lw, T. Pfau, Science **334**, 1110 (2011).
- [26] K.-K. Ni, S. Ospelkaus, M. H. G. de Miranda, A. Pe'er A, B. Neyenhuis, J. J. Zirbel, S. Kotochigova, P. S. Julienne, D. S. Jin, J. Ye, Science **322**, 231 (2008).
- [27] K.-K. Ni, S. Ospelkaus, D. J. Nesbitt, J. Ye, D. S. Jin, Phys. Chem. Chem. Phys. **11**, 9626 (2009).
- [28] K.-K. Ni, S. Ospelkaus, M. H. G. de Miranda, A. Peer, B. Neyenhuis, J. J. Zirbel, S. Kotochigova, P. S. Julienne, D. S. Jin, J. Ye, Science **322**, 231 (2008).
- [29] S. N. Tohme, M. Korek, Chem. Phys. **410**, 37 (2013).
- [30] F. Munchow, C. Bruni, M. Madalinski, A. Gorlitz, Phys. Chem. Chem. Phys. **13**, 18734 (2011).
- [31] M. Borkowski, P. S. Zuchowski, R. Ciurylo, P. S. Julienne, D. Kedziera, L. Mentel, P. Tecmer, F. Munchow, C. Bruni, A. Gorlitz, Phys. Rev. A **88**, 052708 (2013).
- [32] L. K. Sorensen, S. Knecht, T. Fleig, C. M. Marian, J. Chem. Phys. **113**, 12607 (2009); D. A. Brue, J. M. Hutson, Phys. Rev. A **87**, 052709 (2013); M. Tomza, R. Gonzalez-Ferez, C. P. Koch, R. Morzynski, Phys. Rev. Lett. **112**, 113201 (2014).
- [33] F. Herrera, Y. Cao, S. Kais, K. B. Whaley, New J. Phys. **16**, 075001 (2014); M. Karra, K. Sharma, B. Friedrich, S. Kais, D. Herschbach, arxiv:1601.02409.
- [34] A. Micheli, G. K. Brennen, P. Zoller, Nat. Phys. **2**, 341 (2006).
- [35] S. Kotochigova, E. Tiesinga, J. Chem. Phys. **123**, 174304 (2005).
- [36] P. K. Molony, P. D. Gregory, Z. Ji, B. Lu, M. P. Kpinger, C. R. Le Sueur, C. L. Blackley, J. M. Hutson, S. L. Cornish, Phys. Rev. Lett. **113**, 255301 (2014).
- [37] J. Deiglmayr, M. Aymar, R. Wester, M. Weidemller, O. Dulieu, J. Chem. Phys. **129**, 064309 (2008).
- [38] R. Guerout, M. Aymar, O. Dulieu, Phys. Rev. A **82**, 042508 (2010).
- [39] G. Gopakumar, M. Abe, M. Hada1, M. Kajita, J. Chem. Phys. **140**, 224303 (2014).
- [40] R. F. Curl, Mol. Phys. **9**, 585 (1965).
- [41] F. Munchow, PhD thesis, University of Dusseldorf (2012).
- [42] Rb(60s) decay rate has contributions from spontaneous emission with the rate  $\Gamma_{60s}^{sp} = 723$  Hz and from the interaction with black-body radiation at 300 K, which includes BBR induced decay with the rate  $\Gamma_{60s}^{BBR,d} = 0.675\Gamma_{60s}^{sp} = 488$  Hz, excitation to higher Rydberg states with the rate  $\Gamma_{60s}^{BBR,e} = 0.583\Gamma_{60s}^{sp} = 421.5$  Hz, and ionization with the rate  $\Gamma_{60s}^{BBR,ion} = 0.0155\Gamma_{60s}^{sp} = 11.2$  Hz, resulting in the total decay rate  $\Gamma_{60s} = \Gamma_{60s}^{sp} + \Gamma_{60s}^{BBR,d} + \Gamma_{60s}^{BBR,e} + \Gamma_{60s}^{BBR,ion} \approx 1.644$  kHz (V. D. Ovsiannikov, I. L. Glukhov, E. A. Nikipelov, J. Phys. B **44**, 195010 (2011)). Molecular rotational states can also decay due to interaction with black-body radiation, but with much smaller rates  $\sim 10^{-6}$  Hz for the ground vibrational state of KRb at 300 K (S. Kotochigova, E. Tiesinga, P.S. Julienne, Eur. Phys. J. D **31**, 189 (2004)), spontaneous emission decay rates being even smaller.
- [43] D. Jaksch, J. I. Cirac, P. Zoller, S. L. Rolston, R. Cote, M. D. Lukin, Phys. Rev. Lett. **85**, 2208 (2000).
- [44] A. De Pasquale, P. Facchi, Phys. Rev. A **80**, 032102 (2009); B. Olmos, R. Gonzalez-Ferez, I. Lesanovsky, Phys. Rev. Lett. **103**, 185302 (2009); B. Olmos, I. Lesanovsky, Phys. Rev. A **82**, 063404 (2010).
- [45] K. Singer, J. Stanojevic, M. Weidemuller, R. Cote, J. Phys. B **38**, S295 (2005).
- [46] In (a) and (b) thick solid black curve corresponds to the  $|\downarrow, \downarrow, \downarrow\rangle$  state, dashed thick and thin red curves correspond to the  $|\uparrow, \downarrow, \downarrow\rangle$ ,  $|\downarrow, \downarrow, \uparrow\rangle$  and  $|\downarrow, \uparrow, \downarrow\rangle$  states, respectively; dotted thick and thin green curves correspond to the  $|\uparrow, \downarrow, \uparrow\rangle$  and  $|\uparrow, \uparrow, \downarrow\rangle$ ,  $|\downarrow, \uparrow, \uparrow\rangle$  states, respectively, and thick dash-dotted blue curve corresponds to the  $|\uparrow, \uparrow, \uparrow\rangle$  state; In (c) and (d) thick solid black curve corresponds to the  $|\downarrow, \downarrow, \downarrow, \downarrow, \downarrow\rangle$  state, dashed thick, medium and thin red curves correspond to the  $|\uparrow, \downarrow, \downarrow, \downarrow, \downarrow\rangle$ ,  $|\downarrow, \downarrow, \downarrow, \downarrow, \uparrow\rangle$  and  $|\downarrow, \uparrow, \downarrow, \downarrow, \downarrow\rangle$ ,  $|\downarrow, \downarrow, \downarrow, \uparrow, \downarrow\rangle$  and  $|\downarrow, \downarrow, \uparrow, \downarrow, \downarrow\rangle$  states, respectively; dotted green curves in the order of reducing thickness correspond to the  $|\uparrow, \downarrow, \downarrow, \downarrow, \uparrow\rangle$  and  $|\uparrow, \downarrow, \downarrow, \uparrow, \downarrow\rangle$ ,  $|\downarrow, \uparrow, \downarrow, \downarrow, \uparrow\rangle$ ,  $|\uparrow, \downarrow, \uparrow, \downarrow, \downarrow\rangle$  and  $|\downarrow, \downarrow, \downarrow, \uparrow, \uparrow\rangle$ ,  $|\uparrow, \uparrow, \downarrow, \downarrow, \downarrow\rangle$  and  $|\downarrow, \uparrow, \uparrow, \downarrow, \downarrow\rangle$  states, respectively; blue dash-dotted curves in the order of reducing thickness correspond to the  $|\uparrow, \uparrow, \downarrow, \downarrow, \uparrow\rangle$  and  $|\uparrow, \downarrow, \uparrow, \downarrow, \uparrow\rangle$  and  $|\uparrow, \uparrow, \downarrow, \uparrow, \downarrow\rangle$ ,  $|\downarrow, \uparrow, \downarrow, \uparrow, \uparrow\rangle$ ,  $|\uparrow, \downarrow, \uparrow, \uparrow, \downarrow\rangle$ ,  $|\downarrow, \uparrow, \uparrow, \downarrow, \uparrow\rangle$  and  $|\uparrow, \uparrow, \uparrow, \downarrow, \downarrow\rangle$ ,  $|\downarrow, \downarrow, \uparrow, \uparrow, \uparrow\rangle$  and  $|\downarrow, \uparrow, \uparrow, \uparrow, \downarrow\rangle$  states, respectively; thick, medium and thin orange curves correspond to  $|\uparrow, \uparrow, \downarrow, \uparrow, \uparrow\rangle$  and  $|\uparrow, \uparrow, \uparrow, \downarrow, \uparrow\rangle$ ,  $|\uparrow, \downarrow, \uparrow, \uparrow, \uparrow\rangle$  and  $|\downarrow, \uparrow, \uparrow, \uparrow, \uparrow\rangle$ ,  $|\uparrow, \uparrow, \uparrow, \uparrow, \downarrow\rangle$  states, respectively, and thick pink dash-dot-dotted curve corresponds to the  $|\uparrow, \uparrow, \uparrow, \uparrow, \uparrow\rangle$  state.
- [47] C. Weitenberg, M. Endres, J. F. Sherson, M. Cheneau, P. Schau, T. Fukuhara, I. Bloch, S. Kuhr, Nature **471**, 319 (2011).
- [48] R. A. Williams, J. D. Pillet, S. Al-Assam, B. Fletcher, M. Shotton, C. J. Foot, Opt. Expr. **16**, 16977 (2008); S. Al-Assam, R. A. Williams, C. J. Foot, Phys. Rev. A **82**, 021604 (2010).
- [49] Instead of a  $\pi$  pulse one can excite the atom to the Rydberg state using STIRAP (K. Bergmann, H. Theuer, B. W. Shore, Rev. Mod. Phys. **70**, 1003 (1998)) or adiabatic rapid passage (ARP) techniques (E. Kuznetsova, G. Liu, S. Malinovskaya, Phys. Scr. T **160**, 014024 (2014)). Their advantage over a  $\pi$  pulse is that precise tuning of

the pulse area to  $\pi$  is not required, i.e. STIRAP/ARP excitation is robust with respect to pulse duration and Rabi frequency. An additional advantage of ARP excitation is that one does not have to know precisely the shifts of the  $|r\rangle|\uparrow\rangle$  and  $|r\rangle|\downarrow\rangle$  states, provided that the shifts have opposite signs.

- [50] V. B. Braginsky, F. Ya. Khalili, *Rev. Mod. Phys.* **68**, 1, (1996).
- [51] T. C. Ralph, S. D. Bartlett, J. L. O'Brien, G. J. Pryde, H. M. Wiseman, *Phys. Rev. A* **73**, 012113 (2006).
- [52] D. B. Hume, T. Rosenband, D. J. Wineland, *Phys. Rev. Lett.* **99**, 120502 (2007).
- [53] P. Neumann, J. Beck, M. Steiner, F. Rempp, H. Fedder, P. R. Hemmer, J. Wrachtrup, F. Jelezko, *Science* **329**, 542 (2010).
- [54] I. I. Beterov, M. Saffman, *Phys. Rev. A* **92**, 042710 (2015).
- [55] F. Helmer, F. Marquardt, *Phys. Rev. A* **79**, 052328 (2009).
- [56] A. M. Steane, *Proceedings of the International School of Physics "Enrico Fermi"*, edited by G. Casati, D. L. Shepelyansky, P. Zoller, p. 1-32 (IOS Press, Amsterdam, 2006).
- [57] M. Schulte, N. Lorch, I. D. Leroux, P. O. Schmidt, K. Hammerer, arxiv:1501.06453.

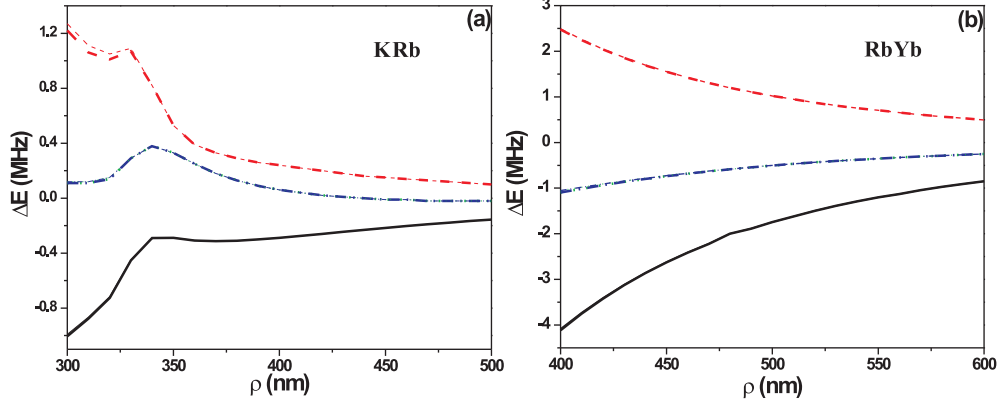


FIG. 2: (a) and (b) Shifts of the  $|60s\rangle |J=0, m_J=0\rangle$  (thick solid black lines),  $|60s\rangle |J=1, m_J=0\rangle$  (thick dashed red lines) and  $|60s\rangle |J=1, m_J=\pm 1\rangle$  (thick dotted blue lines) states of the combined single Rydberg atom-single polar molecule system for KRb and RbYb and Rb, respectively. The atomic basis set included the 60s, 60p, 59p, 59d, 58d and 57f states and the molecular basis set included the  $J=0, 1, 2$  rotational states (full set). The shifts are calculated with respect to unperturbed energies of the states  $E_{ns} + 2BJ(J+1)$ . Thin lines correspond to calculations in which 57f state has not been taken into account.

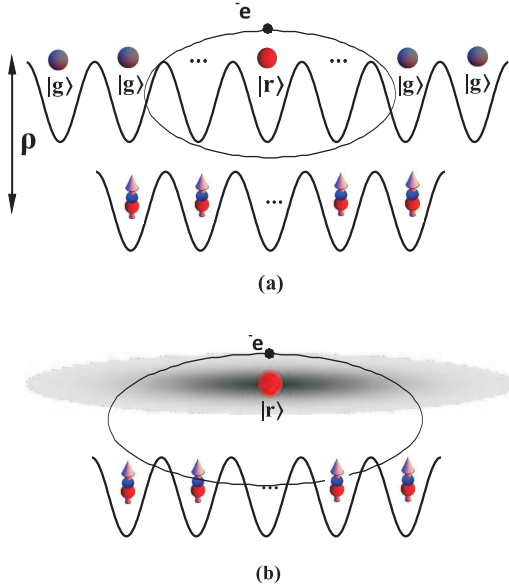


FIG. 3: (a) Schematic of the  $N$  molecular array interacting with an array of  $N_a = N + 2$  atoms. The first and last atoms are added to mitigate the effects of the boundaries. When the atomic system is excited to the 60s state the wavefunction becomes  $|\Psi_{\text{atom}}\rangle = \frac{1}{\sqrt{N_a}} \sum_{j=1}^{N_a} |g_1, \dots, r_j, \dots, g_{N_a}\rangle$ , and each molecule equally interacts with all (most strongly with three nearest) Rydberg atoms; (b) an array of molecules interacting with a cloud of atoms in the superatom state, placed in an elongated dipole trap

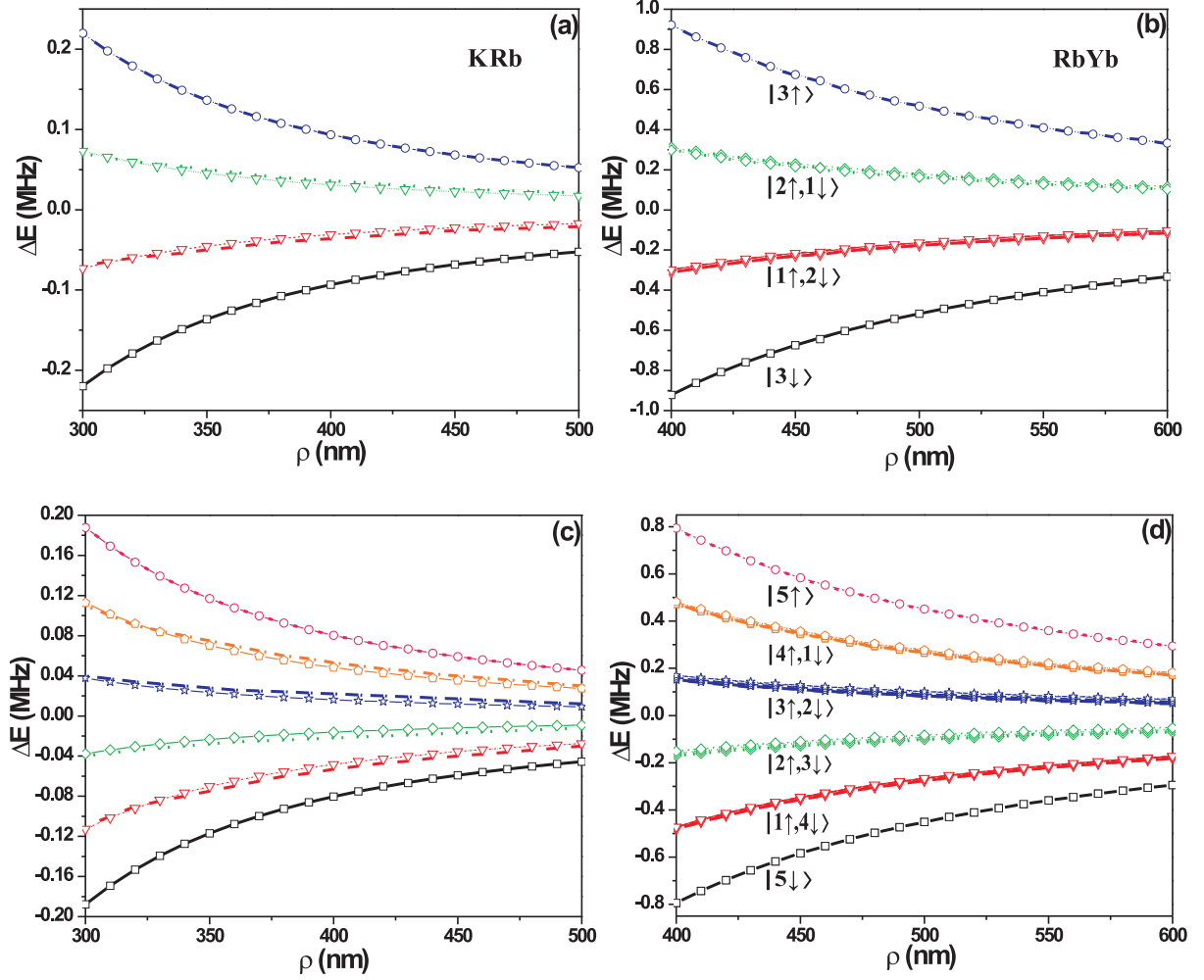


FIG. 4: (a) and (b) Shifts of the states of the combined system of  $N=3$  polar molecules and  $N_a = N+2$  atoms for KRb and RbYb, respectively, and Rb( $60s$ ) calculated by diagonalizing Hamiltonian (5) (lines) and using the perturbation theory expression (7) (open symbols). The atomic system is in the state  $|\Psi_{\text{atom}}\rangle = \frac{1}{\sqrt{N_a}} \sum_{j=1}^{N_a} |g_1, \dots, r_j, \dots, g_{N_1}\rangle$ , and only  $60s$ ,  $|\downarrow\rangle = |J=0, m_J=0\rangle$  and  $|\uparrow\rangle = |J=1, m_J=0\rangle$  atomic and molecular basis states have been used in diagonalizing (5). Solid black line (open squares) correspond to  $|3\downarrow\rangle = |\downarrow, \downarrow, \downarrow\rangle$  state, dashed red lines (open triangles) correspond to single spin up states  $|1\uparrow, 2\downarrow\rangle$ , dotted green lines (open diamonds) correspond to two spins up  $|2\uparrow, 1\downarrow\rangle$  states and a dashed-dotted blue line (open circles) correspond to three spins up  $|3\uparrow\rangle$  state; (c) and (d) the same as in (a) and (b) but for  $N=5$  molecules: solid black line (open squares) correspond to  $|5\downarrow\rangle$  state, dashed red lines (open triangles) correspond to  $|1\uparrow, 4\downarrow\rangle$  states, dotted green lines (open diamonds) correspond to  $|2\uparrow, 3\downarrow\rangle$  states, dash-dotted blue lines (open stars) correspond to  $|3\uparrow, 2\downarrow\rangle$  states, dash-dot-dotted orange lines (open pentagons) correspond to  $|4\uparrow, 1\downarrow\rangle$  states, and short dash pink line (open circles) correspond to the  $|5\uparrow\rangle$  state.

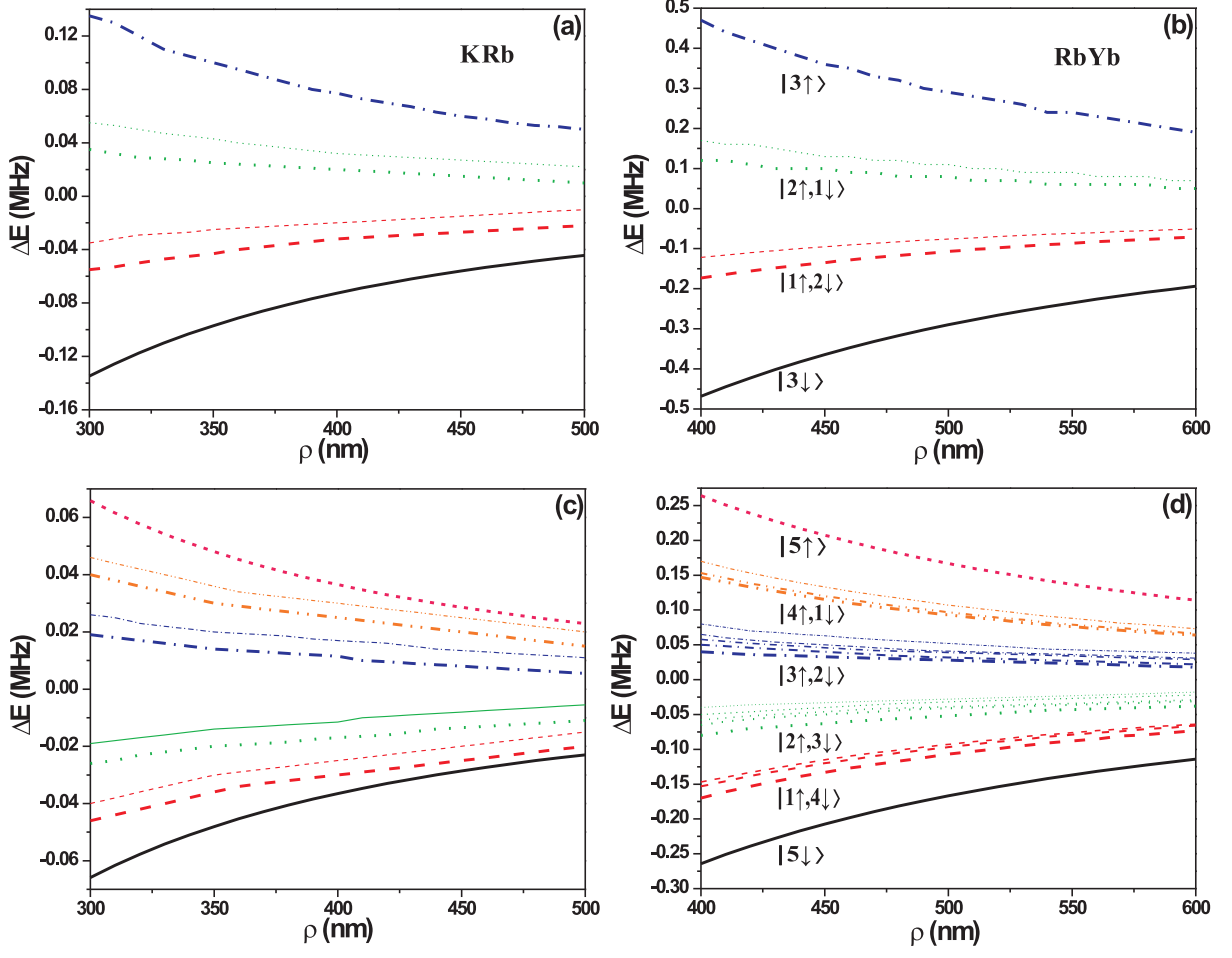


FIG. 5: (a) and (b) Shifts of the states of  $N=3$  polar molecules of KRB and RbYb, respectively, and a Rb superatom in 60s, calculated by diagonalizing the Hamiltonian Eq. (5). The atoms are placed in a 1D Gaussian trap along molecular array with the center of the trap corresponding to the center of the array. The probability to find a single Rydberg atom scales as  $p(x) = \exp(-x^2/a_{\text{trap}}^2)/\sqrt{\pi}a_{\text{trap}}$  along the trap. The trap widths are  $a_{\text{trap}} = 1.3 \mu\text{m}$  and  $a_{\text{trap}} = 1.7 \mu\text{m}$  for KRB and RbYb, respectively. (c) and (d) shifts of collective states for  $N = 5$  molecules of KRB and RbYb, respectively. The trap widths are  $a_{\text{trap}} = 2.5 \mu\text{m}$  for KRB and  $a_{\text{trap}} = 3 \mu\text{m}$  for RbYb. Collective rotational states are denoted similarly to Fig. 4 (detailed description is given in [46]).

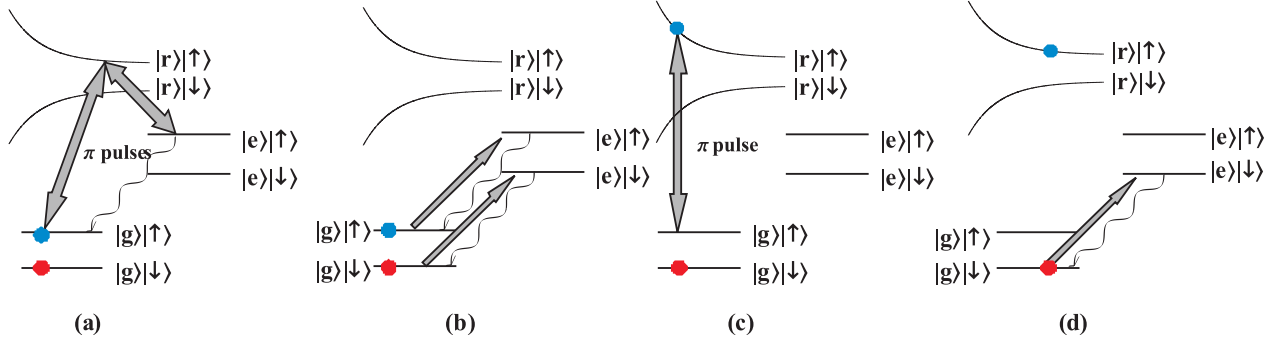


FIG. 6: Readout of populations of molecular rotational states  $|\downarrow\rangle = |J=0, m_J=0\rangle$  and  $|\uparrow\rangle = |J=1, m_J=0, \pm 1\rangle$ . (a) Population of the  $|\uparrow\rangle$  state can be measured by selectively exciting the atom-molecule system to the  $|r\rangle|\uparrow\rangle$  state by a  $\pi$  pulse, followed by transfer by a second  $\pi$  pulse to some  $|e\rangle|\uparrow\rangle$  state, rapidly decaying to the  $|g\rangle|\uparrow\rangle$  state. The transfer  $|g\rangle|\uparrow\rangle \rightarrow |r\rangle|\uparrow\rangle \rightarrow |e\rangle|\uparrow\rangle$  can be also done using STIRAP or ARP. The population of the  $|g\rangle|\downarrow\rangle$  can be read out in a similar way; (b) While the atom is in the ground state and does not interact with the molecule atomic fluorescence intensity can be measured using excitation and deexcitation on a cycling transition  $|g\rangle \leftrightarrow |e\rangle$ ; (c) The combined system can be conditionally transferred from the  $|g\rangle|\uparrow\rangle$  to the  $|r\rangle|\uparrow\rangle$  state via a  $\pi$  pulse or an ARP pulse; (d) Atomic fluorescence intensity on the  $|g\rangle \leftrightarrow |e\rangle$  transition is measured again. The difference between the fluorescence intensities before and after the Rydberg excitation allows to obtain populations of the rotational states.

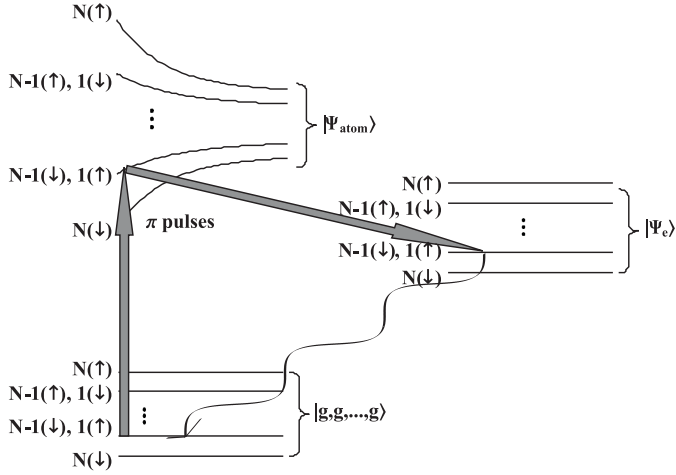


FIG. 7: Schematic of measurement of populations of collective states with a certain number of molecular spins up and down.

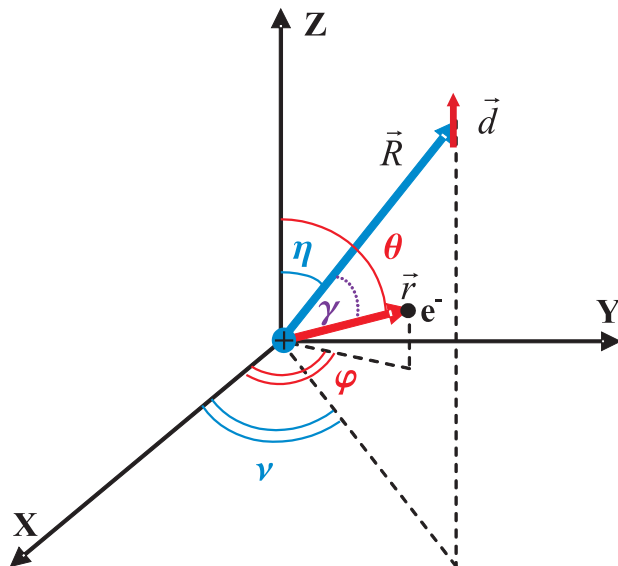


FIG. 8: Angles of the vectors  $\vec{R}$  and  $\vec{r}$  in the case of a general orientation of the Rydberg atom with respect to the molecule.

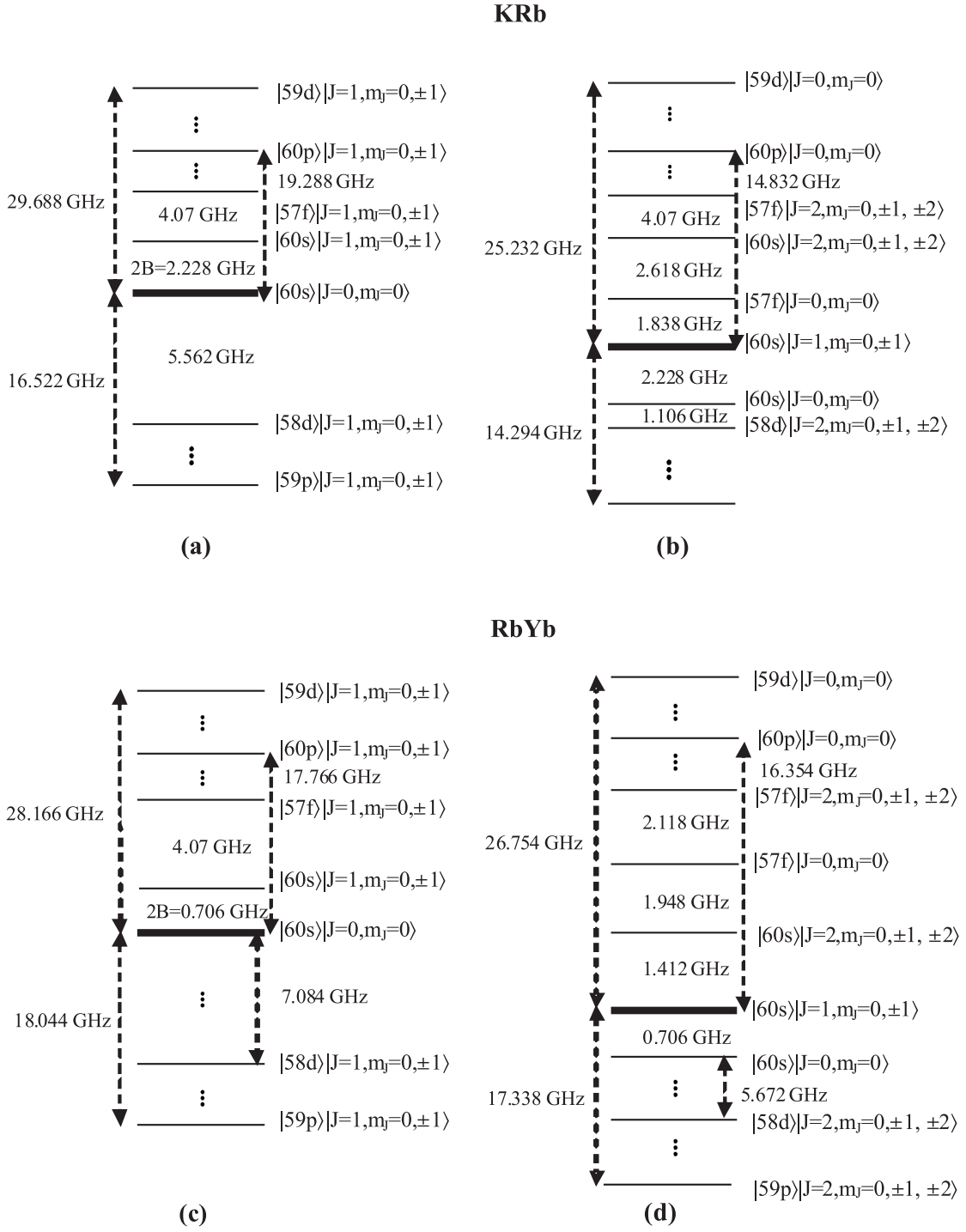


FIG. 9: Schematic of the states closest to the qubit states  $|\downarrow\rangle = |ns\rangle |J=0, m_J=0\rangle$  and  $|\uparrow\rangle = |ns\rangle |J=1, m_J=0, \pm 1\rangle$  with the corresponding energies.

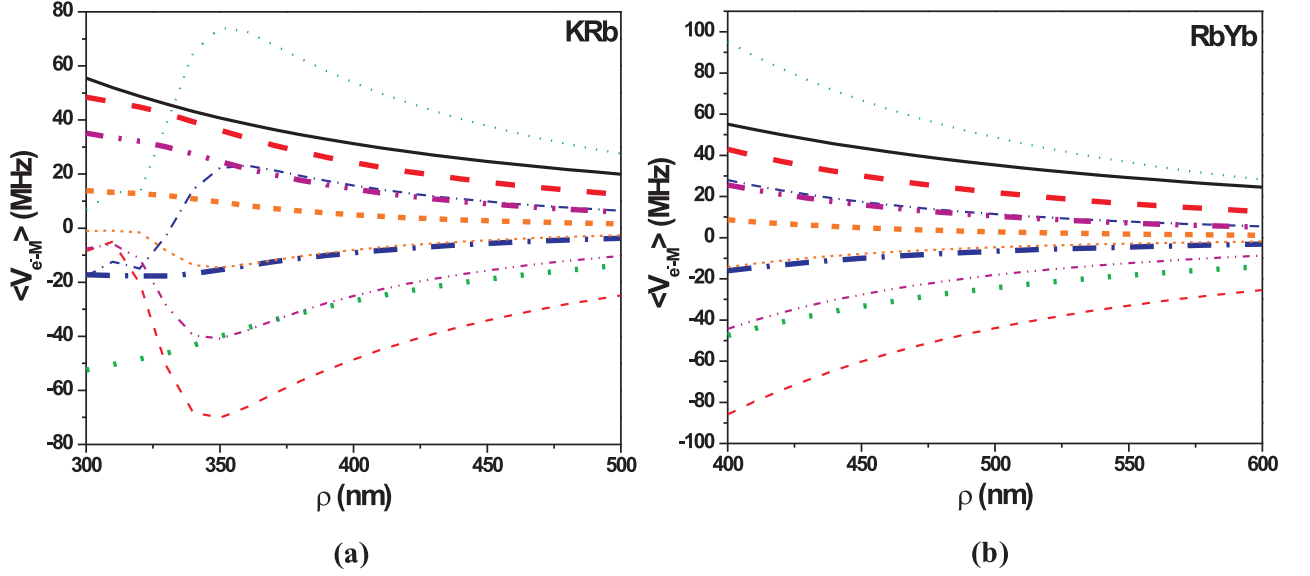


FIG. 10: Interaction matrix elements, most relevant to the energy shifts of the  $|ns\rangle|\uparrow\rangle$ ,  $|ns\rangle|\downarrow\rangle$  states:  $\langle V_{e-M} \rangle = \langle ns | \langle J=0, m_J=0 | V_{e-M} | n'l'm' \rangle | J'=1, m'_J \rangle$ , where  $m'_J + m' = 0$ . The curves correspond to  $|n'l'm' \rangle | J'=1, m'_J \rangle = |ns \rangle | J'=1, m'_J=0 \rangle$  (solid black line),  $|np, m'=-1 \rangle | J'=1, m'_J=1 \rangle$  (thick dashed red line),  $|np, m'=0 \rangle | J'=1, m'_J=0 \rangle$  (thin dashed red line),  $|(n-1)p, m'=-1 \rangle | J'=1, m'_J=1 \rangle$  (thick dotted green line),  $|(n-1)p, m'=0 \rangle | J'=1, m'_J=0 \rangle$  (thin dotted green line),  $|(n-1)d, m'=-1 \rangle | J'=1, m'_J=1 \rangle$  (thick dash-dotted blue line),  $|(n-1)d, m'=0 \rangle | J'=1, m'_J=0 \rangle$  (thin dash-dotted blue line),  $|(n-2)d, m'=-1 \rangle | J'=1, m'_J=1 \rangle$  (thick dash-dot-dotted magenta line),  $|(n-2)d, m'=0 \rangle | J'=1, m'_J=0 \rangle$  (thin dash-dot-dotted magenta line),  $|(n-3)f, m'=-1 \rangle | J'=1, m'_J=1 \rangle$  (thick short-dashed orange line), and  $|(n-3)f, m'=0 \rangle | J'=1, m'_J=0 \rangle$  (thin short-dashed orange line).

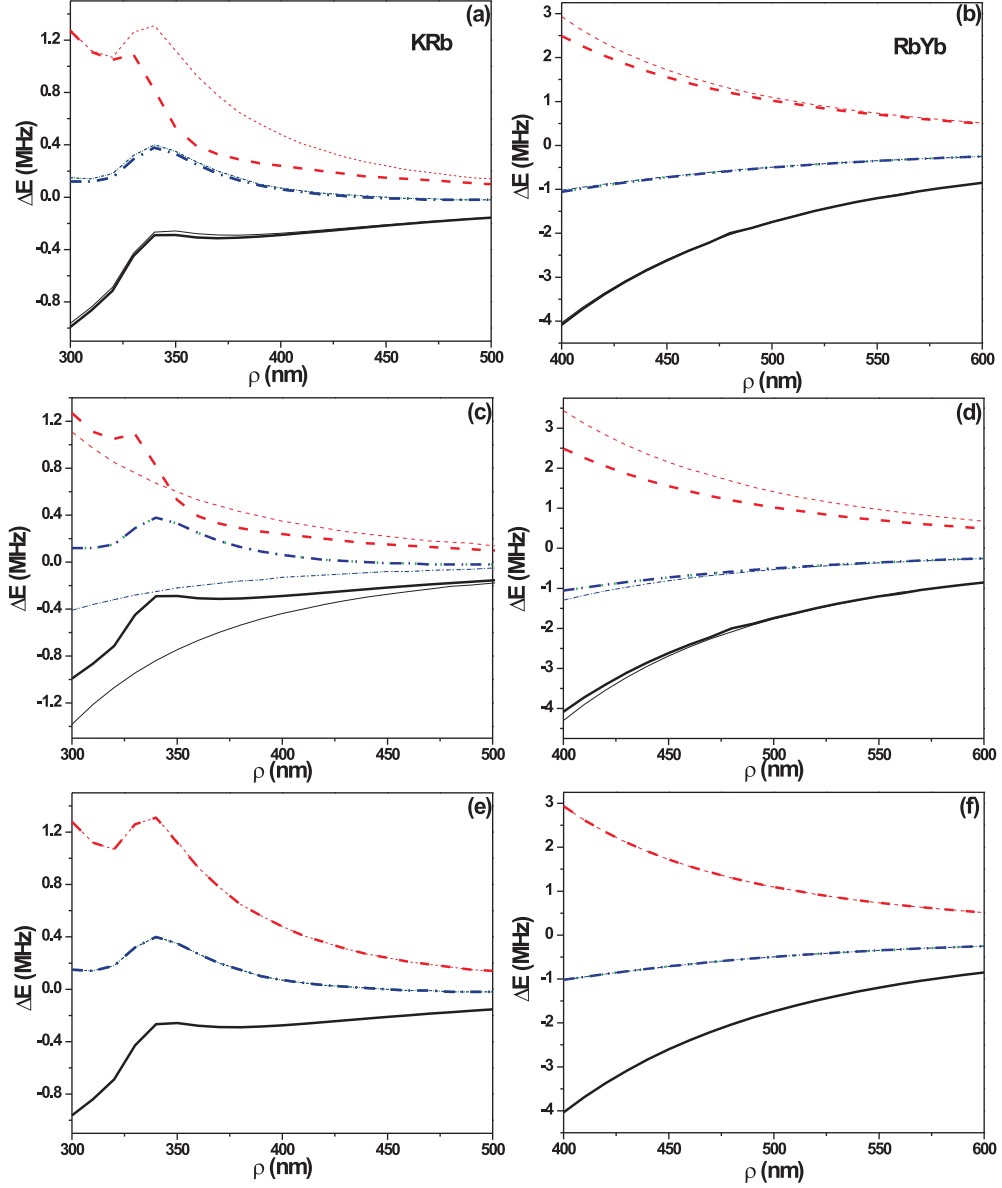


FIG. 11: (a) and (b) Shifts of the  $|ns\rangle|J=0, m_J=0\rangle$  (solid black lines),  $|ns\rangle|J=1, m_J=0\rangle$  (dashed red lines) and  $|ns\rangle|J=1, m_J=\pm 1\rangle$  (dotted blue lines) states of the combined single Rydberg atom-single polar molecule system for KRb and RbYb and Rb, respectively. The shifts are calculated with respect to unperturbed energies of the states  $E_{ns} + 2BJ(J+1)$ . The atomic basis set included the  $60s$ ,  $60p$ ,  $59p$ ,  $59d$ ,  $58d$  and  $57f$  states and the molecular basis set included the  $J=0, 1, 2$  rotational states (thick lines). Thin lines correspond to calculations in which a smaller atomic basis set of  $60s$ ,  $60p$ ,  $59p$  and  $58d$  was used; In (c) and (d) the full shifts (thick lines) are compared to the shifts calculated using the smallest atomic basis set of  $60s$  (thin lines); in (e) and (f) the shifts calculated using the smaller atomic basis set of  $60s$ ,  $60p$ ,  $59p$ ,  $58d$  and  $J=0, 1, 2$  rotational states (thick lines) are compared to the shifts calculated using  $J=0, 1, 2, 3$  rotational states (thin lines).